Chapter III

Photo-induced electron transfer in type I (Fe-S type) photosynthetic reaction center of heliobacteria

Chapter introduction

Photosynthesis

Photosynthesis produces carbohydrate essential for living organisms. The carbohydrate is synthesized via two processes [1]; the first is the energy conversion of light energy into chemical energy, i.e. production of adenosine triphosphate (ATP) and reduced nicotinamide adenine dinucleotide phosphate (NADPH) or reduced nicotinamide adenine dinucleotide (NADH), and the second is the carbon dioxide fixation through Calvin cycle consuming the ATP and the NADPH or NADH. The first light-to-chemical energy conversion occurs in thylakoid membrane of chloroplast and cyanobacteria (or in plasma membrane in the case of anoxygenic photosynthetic bacteria). The membranes separate a small cavity from the outside environment, in which the inner cavity and the outside region called thylakoid lumen and stroma, respectively, in chloroplast and cyanobacteria. Various protein complexes are embedded in the biological membrane and function as pumps of electron and proton. In oxygenic photosynthesis of higher plants, algae, and cyanobacteria, the primary reactions are carried out mainly in four protein complexes; photosystem I and II (PS I and II), cytochrome complex, and ATP synthase (Fig.III-1). The reaction process until production of ATP and NADPH is generally divided into three steps; (1) Light energy captured by photosynthetic pigments in PS I or PS II is transferred to its reaction center (RC) protein complex, leading to charge separation in the RC. (2) The photo-induced electron is transferred across the membrane through PS I RC, PS II RC, or cytochrome complex (Fig.III-1). The transmembrane electron transfer induces proton transport across the membrane, resulting in difference in electrochemical potential (i.e. proton-motive force). (3) The potential difference drives transmembrane proton transfer through the ATP synthase, accompanied by stepwise rotations of the molecular motor in the ATP synthase that promotes the synthesis of ATP from ADP.

Functions of photosynthetic RC

Photosynthetic RC serves as the reaction field for the light-to-chemical energy conversion process in photosynthesis. Pigment molecules and metal clusters are embedded in the RC complex and mediate the electron transfer, in which the protein scaffold optimizes relative arrangement and redox potential of the cofactors. X-ray structural analysis has revealed a lot of crystal structures of RC complex since the crystal structure of purple bacterial RC had been solved in 1985 (Fig.III-2A) [2]. RC complex is classified into two types according to the terminal electron acceptor; type I and II RCs. Type I RC employs iron sulfur (Fe-S) clusters at the terminal of the electron transfer pathway, hence it is also referred to as “Fe-S type RC”. Type II RC utilizes quinone (Q) molecules as the terminal electron acceptor, and is also called “Q type RC”.

Oxygenic photosynthetic organisms possess both the type I and II RCs, which is PS I and PS II RCs, respectively (Fig.III-2B). Light excitation induces charge separation and sequential electron transfer in PS II RC. The ejected electron is transferred to the terminal mobile quinone (Q_B) on the stromal side via another binding quinone (Q_A), in which the Q_B receives two electrons with two protons and then is released to quinone pool. The cation induced in the charge separation, which remains on the lumenal side of PS II RC, decays with charge recombination with the electron provided from manganese cluster. The metal cluster catalyzes oxidation of stable water molecule and excretes oxygen and proton. Light-driven electron transfer also occurs in PS I RC. The photo-induced electron is transferred to the terminal Fe-S clusters (F_X, F_A, and F_B) via quinone molecules (A_1). Then, ferredoxin (F_d) that is a soluble electron carrier is reduced, following by reduction of $NADP^+$ to NADPH with ferredoxin-$NADP^+$ oxidoreductase (FNR) in stromal region. The electron from PS II RC though cytochrome *b*$_6$*f* complex and plastocyanin (PC) cancels the cation left on the lumenal side of PS I RC. PS II and PS I RCs, which are connected in series, generate the vectorial light-driven electron transfer and consequently produce a voltage potential difference of more than 1 V as a battery, in which the RCs serve as a cathode and a anode, respectively. Although the PS II and PS I RCs collaborate in oxygenic photosynthesis, they seem to originate from distinct RCs; RC II and RC I, respectively. The RC II is the Q type RC seen in purple bacteria and green filamentous bacteria, while the RC I is the Fe-S type RC seen in heliobacteria and green sulfur bacteria.

Structure of RC complex

All known RCs form dimeric structure consisting of two transmembrane core polypeptides. Each polypeptide contains electron transfer mediators such as chlorophyll (Chl) and quinone molecules, and the RC produces significantly symmetrical electron transfer pathway (Fig.III-2A). Photo-induced electron is sequentially transferred via these cofactors along the pathway (Fig.III-2C). RC II, PS II RC, and PS I RC form a heterodimeric structure consisting of similar but different two core polypeptides, which are called L/M, D1/D2, and PsaA/PsaB, respectively. PS II RC, whose D1/D2 subunits have low similarity (~30%), exhibits complete asymmetric (unidirectional) electron transfer along the D1 branch. The asymmetric property of D1 and D2 is strongly reflected in functions of quinone molecules Q_A and Q_B, which are binding and mobile quinines, respectively. Two-electron-reduced Q_B readily exchanges with oxidized one in the quinone pool and serves as an electron/proton carrier. Meanwhile, Q_A is proposed to change the orientation of its head group when receiving an electron and to control the electron transfer rate from Q_A to Q_B as reported in RC II (Fig.III-3) [3]. The reorientation of Q_A would alter the exchange coupling between Q_A and Q_B, which is a factor determining the electron transfer rate [4]. PsaA/PsaB subunits in PS I RC have somewhat higher similarity (~50%), and both quinone-A_1 molecules in PsaA (A_{1A}) and PsaB subunits

(A_{1B}) bind tightly to the protein scaffold. The similarity allows the electron to pass through both branches along PsaA and PsaB, while the bidirectional electron transfer is not entirely symmetric. The electron transfer rate from A_{1B} to F_X is about ten times faster than that from A_{1A} to F_X, indicating different property between A_{1B} and A_{1A} [5]. Although the importance of the broken symmetry of the two electron transfer pathways in RC is still unclear, the asymmetrical pathway seems to be essential to efficiency of the heterodimeric RC.

In contrast to the heterodimeric RCs (PS I and PS II RCs and RC II), only RC I of heliobacteria and green sulfur bacteria exhibits homodimeric form that consists of two identical polypeptides, and thus the symmetrical electron transfer is expected to occur in RC I. An evolutionary model based on protein homology of RC suggests that an ancestral homodimeric RC had changed into all contemporary RCs including type I and II RCs (Fig.III-4) [6,7], although there are various hypothetical models for evolution of RC. Therefore, the persisting homodimeric RC I is proposed to reflect properties of the ancestral RC and to give a clue to the elucidation of evolution process from homodimer to heterodimer and from type I RC to type II RC. Especially, the function of quinone molecules in RC I seem to be fundamental to discuss the issues because the quinone function is expected to affect the functional symmetry of RC as known in the heterodimeric RCs. In addition, F_X cofactor would also be sensitive to the dimeric structure of RC because it locates at the center between two subunits of the RC. However, the crystal structure of RC I is unsolved at present, and A_1 and F_X cofactors in the RC are not well understood as stated below.

Heliobacterial RC

Heliobacteria is anoxygenic photosynthesis organism discovered in 1983 [8], and usually found in soil habitats such as paddy fields and hot springs [9]. They closely related to cyanobacteria based on analyses of their 16S rRNA sequence [10] and photosynthesis gene [11]. The heliobacterial RC (hRC) was identified as a homodimeric RC I (Fe-S type RC) consisting of two identical core polypeptides PshA [12-14] as green sulfur bacterial RC (gRC) consisting of two PscA subunits [15]. The symmetrical RC structure predicts that an electron passes evenly through both branches. Major pigment in hRC is BChl *g* that exhibits the Q_y absorption peak at 800 nm, which is found only in heliobacteria (Fig.III-5). BChl *g* is instantly oxidized to Chl *a*-like pigment in aerobic environment because of the extreme sensitivity to oxygen, resulting in the loss of photochemical activity of hRC. This isomerization changes the color of the pigment from brownish-green to emerald-green. hRC has a small size of antenna composed of 35-40 BChl *g* molecules and is associated with no light-harvesting antenna protein complexes [16]. The simplified photosynthetic system is obviously different from other RCs including huge antenna systems and even another homodimeric gRC which

have large amounts of antenna pigments in huge antenna complexes, called chromosomes and FMO, attached to the RC surface (Fig.III-6) [17,18].

The amino acid sequence analysis suggested that the electron transfer cofactors were bound to PshA in analogy to their counterparts in PS I RC (Fig.III-2) [19]. Light energy absorbed by the antenna pigments is transferred to the special pair P800 which is a dimer made of BChl g' (or a heterodimer of BChl g and g') [20,21], followed by the charge separation to the primary electron acceptor A_0 which is a derivative of Chl *a*, 8^1-hydroxy-Chl *a* (8^1-OH-Chl a) [16,22]. The sequential electron transfer separated along two branches finishes on terminal electron acceptors F_A/F_B which are [4Fe-4S] clusters ligated within a PshB protein similar to PsaC in PS I or PscB in green sulfur bacteria [23]. In the case of PS I RCs, phylloquinone A_1 and iron sulfur cluster F_X are known to function as a secondary and a tertiary electron acceptor, respectively, between A_0 and F_A/F_B (Fig.III-2A). On the other hand, the property of F_X has not been defined in the hRC, and it is still under debate whether or not the RC has functional quinone-A_1 molecules [24,25].

Unidentified cofactor in hRC; Fe-S cluster F_X

The iron sulfur cluster F_X was expected to be located at the center as the junction of the core protein complex formed by two PshA subunits, in which each PshA provided two cysteine residues known as a ligand of iron sulfur clusters in PS I (Fig.III-7) [14] in a manner analogous to the PscA/PscA homodimeric RC of green sulfur bacteria [17]. Amino acid sequences of the F_X-binding site are highly conserved (~50 %) in hRC and PS I RC [26]. In contrast with the anticipation of a functional F_X in hRC, it had been undetectable by both optical and EPR measurements for a long time. Transient absorption experiments exhibited that the charge recombination of $P800^+$ proceeded with a time constant of 14 ms in hRC complex at room temperature [12]. The absorption change at 430 nm was accompanied by the decay of $P800^+$ with a time constant of 20 ms, interpreted as the charge recombination between $P800^+$ and F_X^- [27]. Moreover, a Fe-S cluster EPR signal exhibiting a conventional spin state of $S = 1/2$ was assigned to F_X [26]. On the other hand, another EPR signal attributed to F_X with an $S = 3/2$ ground spin state was also reported [28]. These incompatible results created a controversy about properties of F_X in heliobacteria.

Unidentified cofactor in hRC; menaquinone A_1

Phylloquinone serves as a secondary electron acceptor A_1 in PS I RC, in which the A_1 molecule binds to hydrophobic pocket. The amino acid sequence of PshA of hRC indicates the presence of A_1-binding site, exhibiting high similarity (~50%) to that in PS I RC in spite of lower similarity (10~15%) of whole RC core subunit between the two species [26]. The homology model based on the sequence similarity suggests that the A_1-binding site in hRC is more hydrophilic than that

in PS I RC because several neutral amino acid residues in PS I RC are replaced by charged residues in hRC (Fig.III-8). The hydrophilic nature results in the weak binding of A_1 to the protein scaffold. It has even been suggested that reduced quinones exchange with oxidized ones in the quinone pool within membrane as mobile quinines (Q_B) in PS II RC and RC II [17,29]. The quantity of menaquinone was evaluated at 1.4 molecules per P800 in hRC [12]. On the other hand, functional menaquinone A_1, i.e. transient photo-induced menaquinone radical, has not been properly identified in hRC by neither optical nor EPR measurements. To date, various studies indicating the absence or presence of the functional A_1 were reported as below, and it has been controversial whether or not menaquinone serves as electron mediator A_1 in hRC.

The reoxidation of A_0^- formed in the primary charge separation was assumed to proceed with 500-600 ps at room temperature in heliobacteria [30,31] and green sulfur bacteria [32], which was considerably slower than that of 20-50 ps for the reoxidation of A_0^- via phylloquinone-A_1 in PS I [33,34]. No transient absorption change was detected in the 400-470 nm region where A_1^- signal is observed [30]. Only one signal ascribed to $P800^+F_X^-$ state was observed at 100 K by time-resolved ESR measurements, in contrast to the case of PS I RC where two signals of $P700^+A_1^-$ and $P700^+F_X^-$ were observed [35]. Photovoltage measurements indicated that only two steps occurred in the electron transfer following a laser flash in hRC, while three steps, $P700 \rightarrow A_0 \rightarrow A_1 \rightarrow F_X$, occurred in PS I RC [36]. Therefore, it assumed that the intermediate electron acceptor A_1 was missing in hRC. Despite of extraction of phylloquinones-A_1 from PS I with diethyl ether treatment, no changes was found in the reoxidation rate of A_0^- [37]. These results suggest the electron transfer directly from A_0 to F_X in hRC. On the other hand, EPR and ENDOR studies showed that semiquinone radical can be photoaccumulated [38,39]. The charge recombination kinetics obtained in transient absorption spectra around 800 nm at 10 K was separated into two phase which were attributed to two different electron acceptors A_1 and F_X [40]. The redox titration of hRC core complex without a PshB subunit containing F_A/F_B clusters suggested the existence of two different electron transfer cofactors, i.e. A_1 and F_X, following A_0 [41]. These results imply the presence of functional A_1 in hRC as in PS I RC.

Outline of this chapter

I determined the precise orientations of multiple iron sulfur centers in hRC from the angular dependence of EPR signals of the clusters detected in the oriented membranes of *Hbt. modesticaldum*. The orientation of "S = 1/2 F_X^- type signal" was comparable to that of F_X^- in PS I RC, suggesting that the signal is assigned to F_X in an S = 1/2 spin state. The F_X signal indicates more symmetric structure of F_X in hRC than that in PS I and gRC. The high symmetry of F_X seems to reflect the simplified and homodimeric structure of hRC, in contrast to the heterodimeric PS I RC and the homodimeric, but complicated gRC (Fig.III-6). The rapid decay kinetics of F_X^- in hRC even at cryogenic temperature

was also different from that in PS I. In addition, the orientation of F_B^- in hRC was very similar to that of F_A^- in PS I RC. It seems that the electron transfer chain on the reducing side of hRC resembles that of PSI with little different EPR and kinetic features of iron sulfur clusters.

In order to characterize quinone-A_1, a photo-induced radical pair of electron donor $P700^+$ and A_1^- has been detected by time-resolved (TR) EPR spectroscopy [42]. The radical pair is induced in the ultra-fast electron transfer process, thus maintains the electron spin polarized (ESP) state that is unique energy state distinct from Boltzmann distribution (see General Introduction). The $P700^+A_1^-$ radical pair in the ESP state produces a typical EPR signal reflecting relative arrangement of the radicals. In hRC, however, only $P800^+F_X^-$ radical pair has been detected and the $P800^+A_1^-$ radical pair is undetectable, in contrast to PS I RC where the $P700^+A_1^-$ pair is usually detected below 150 K. Therefore, I chemically pre-reduced the terminal electron acceptor F_X in hRC, and detected the $P800^+A_1^-$ radical pair. The spectral pattern of the ESP signal was obviously different from that of $P700^+A_1^-$ signal in PS I RC. Based on the spectral simulation, the molecular orientation of A_1 in hRC was proposed to be different from that in PS I RC. The time constant of the charge recombination between $P800^+$ and A_1^- changed somewhat depending on temperature, which is also different from the situation in PS I RC. These results suggest that quinone-A_1 mediates the electron transfer between the electron acceptor A_0 and F_X in hRC as A_1 in PSI RC, but with a little different manner.

Figures

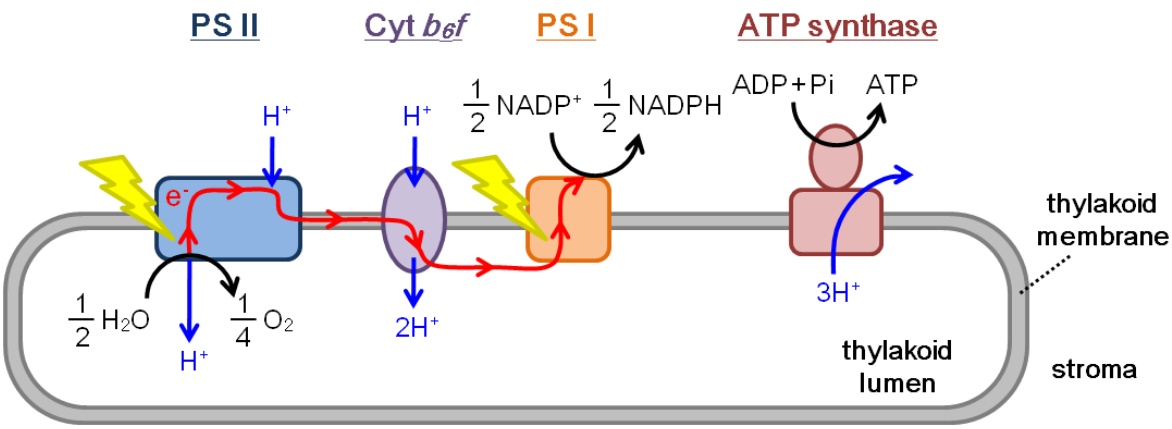

Figure III-1: Schematic model of light-driven electron transfer associated with proton transport from stromal region to thylakoid lumen in chloroplast and cyanobacteria. The electron transfer and proton transport are indicated by a red arrow and blue arrows, respectively.

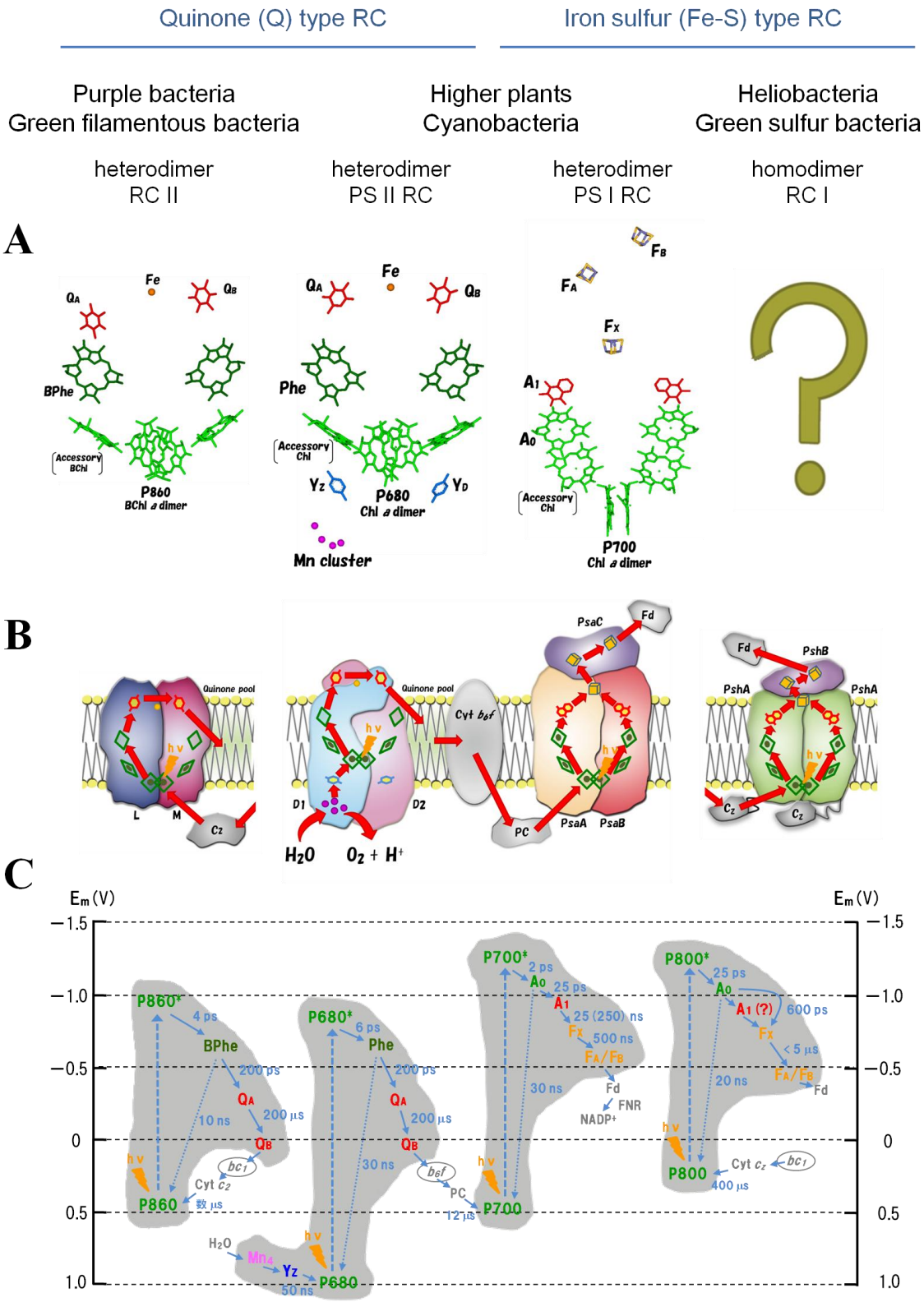

Figure III-2: 4 type RC complexes. (A). X-ray crystal structures of RC II, PS II RC, and PS I RC (PDB entry 1RZH, 2AXT, and 1JB0, respectively). Crystal structure of RC I is still unclear. (B). Electron transfer pathways in the RC. The electron transfer pathways are indicated by red arrows. (C). Electron transfer rate between cofactors in the RC [43]. The vertical axis represents redox potential.

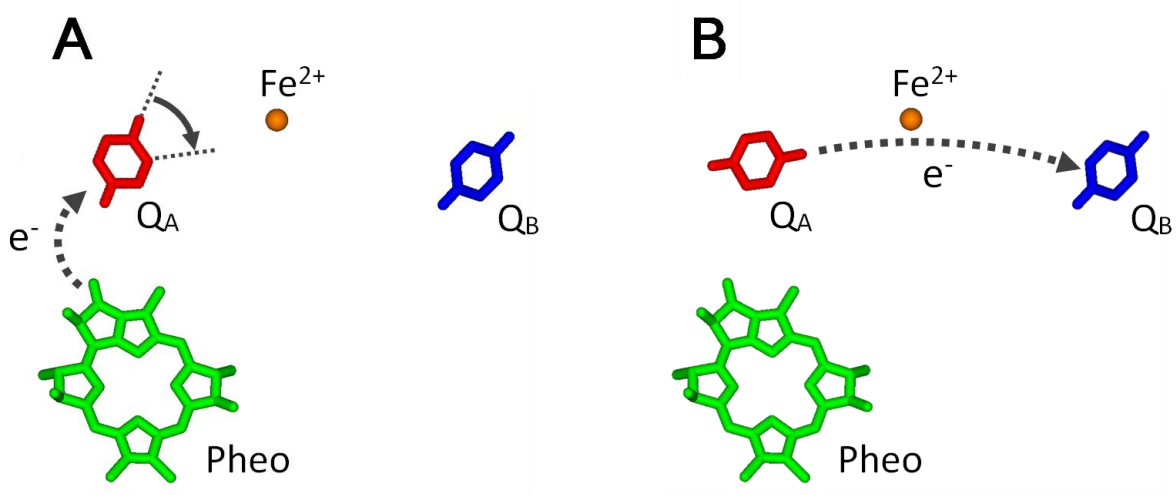

Figure III-3: Gating step of the electron transfer from Q_A to Q_B through a 60° rotation of Q_A when receiving an electron. The model was proposed in RC II based on the EPR study [3]. Spatial arrangement of Q_A^- in (A) an inactive state where the electron transfer to Q_B is impaired and (B) an active configuration allowing the electron transfer are shown. Pheo indicates bacteriopheophytin serving as an electron acceptor in RC II. The dotted arrows indicate electron transfer steps. The solid arrow indicates the gating step that is a 60° rotation of Q_A.

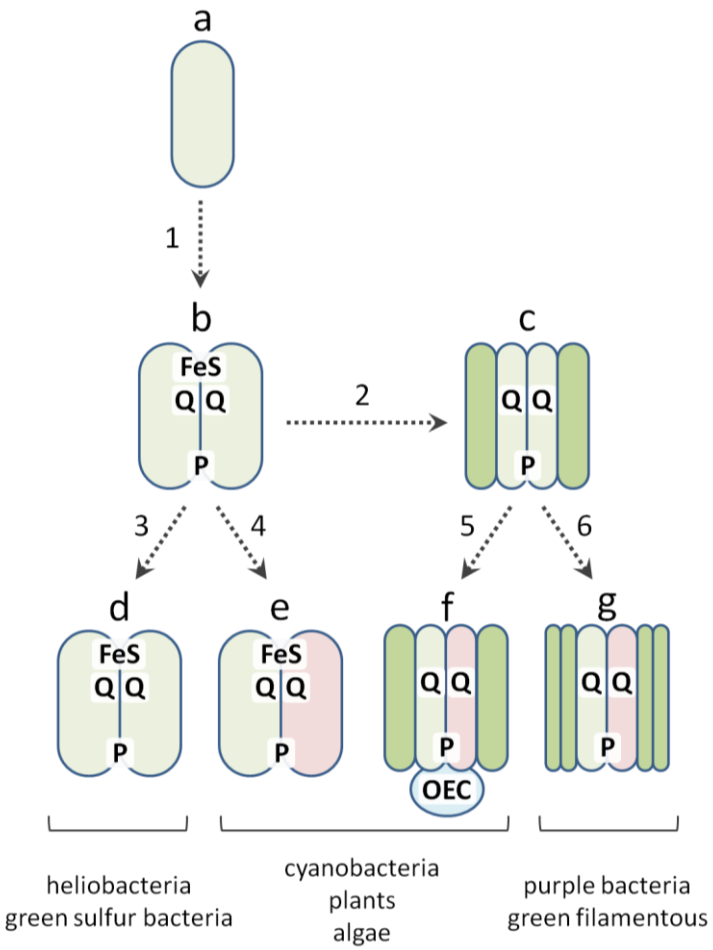

Figure III-4: Evolutionary model of RC based on the protein homology [6]. First of all, the ancestral homodimeric RC I (defined as *b*) was generated. The next evolutionary changes (step 2) were the loss of Fe-S clusters and the splitting of one large subunit gene into two smaller genes, in which one codes for an antenna complex (shadow area) and the other for homodimeric ancestral RC II (defined as *c*). In steps 4 and 5, a gene duplication and divergence in the ancestral RC I and RC II resulted in heterodimeric PS I RC consisting of PsaA/PsaB subunits and PS II RC consisting of D1/D2 subunits, respectively (defined as *e* and *f*). The evolutionary steps took place only in the cyanobacteria. The heterodimeric RC II consisting of L/M subunits (defined as *g*) evolved from the ancestral RC II (step 6). In the process, the antenna complex split into two components. The homodimeric RC I (defined as *d*) evolved from the ancestral RC I (step 3), and seems to conserve properties of the primitive RC.

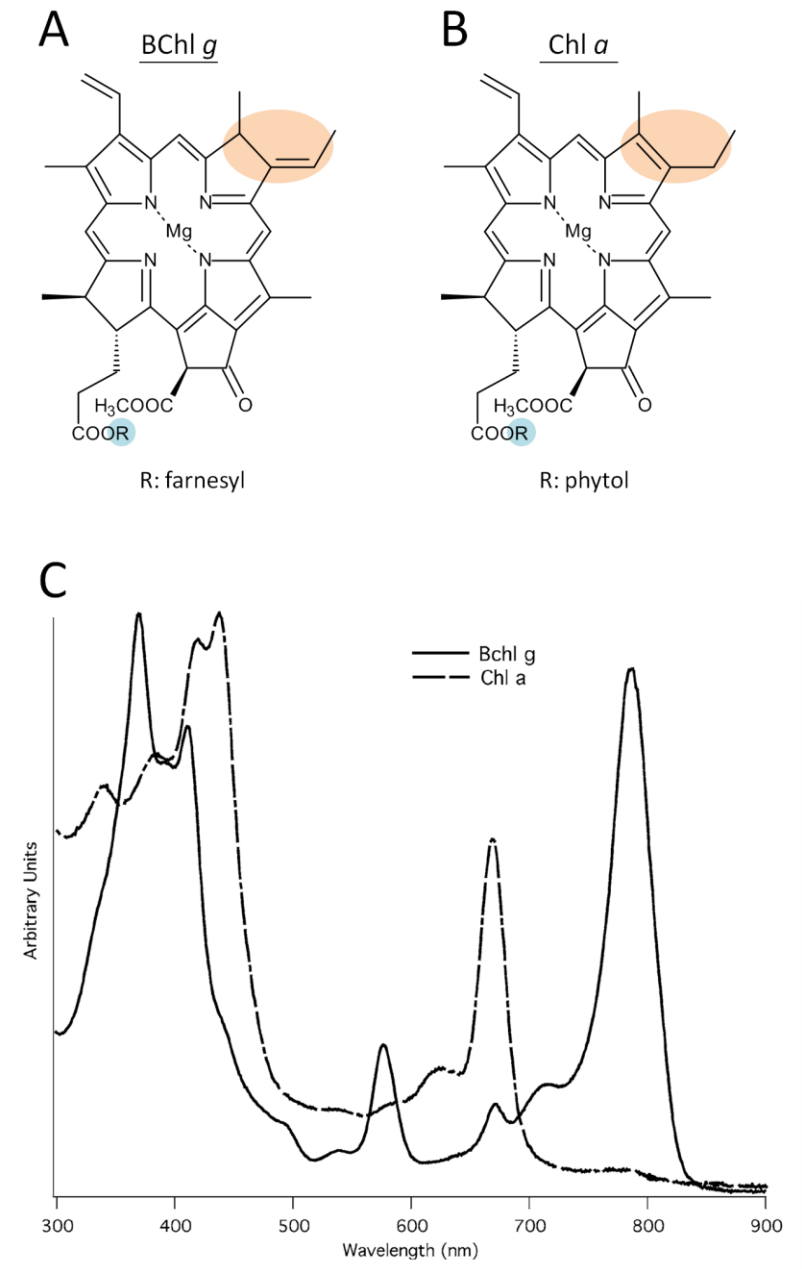

Figure III-5: Molecular structures of (A) BChl *g* and (B) Chl *a*. Structural differences between the two pigments are highlighted in orange and blue. In the presence of oxygen and light, BChl *g* is oxidized to Chl *a*-like pigment, in which C7=C8 double bond is formed on ring II as highlighted in orange. (C). Absorption spectra of BChl g (solid line) and Chl a-like pigment that is BChl *g* after a 2 hour exposure to light and oxygen (broken line). (The figure C was quoted from [25])

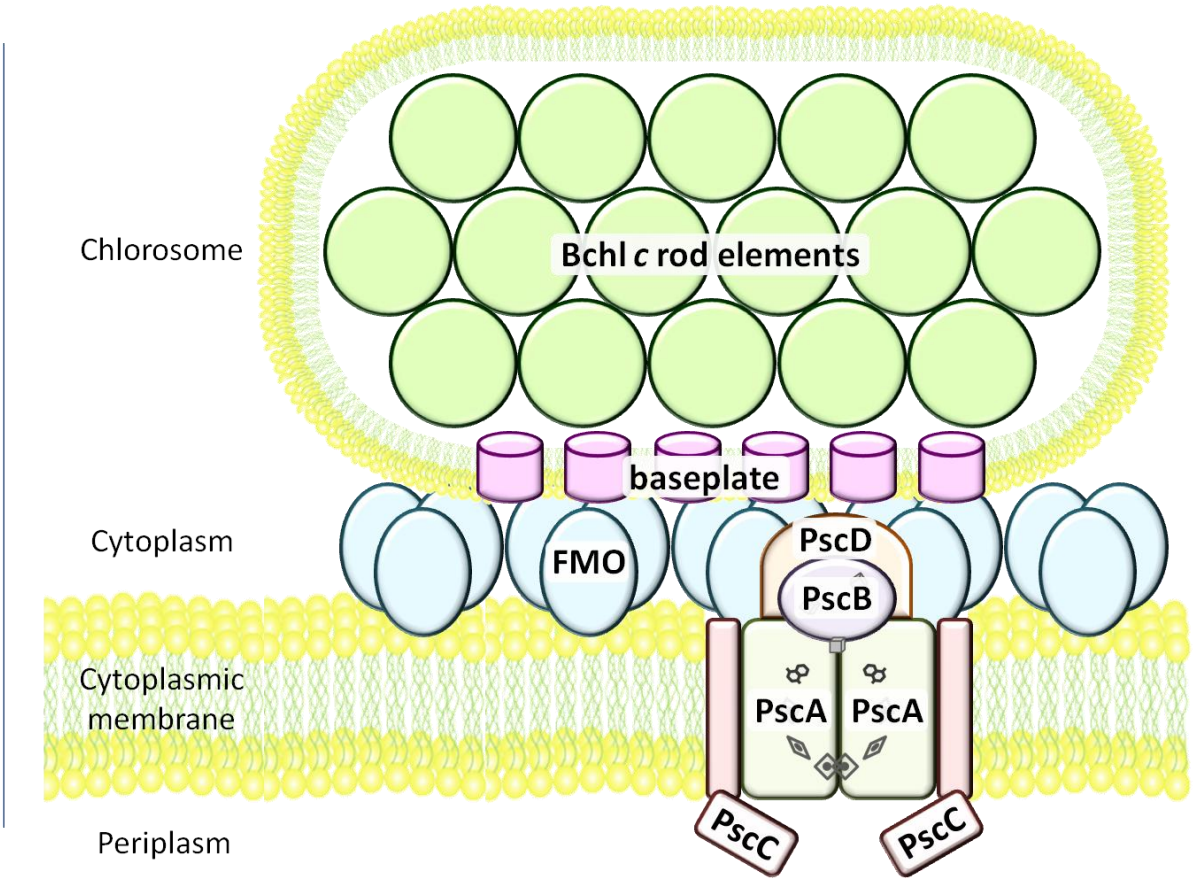

Figure III-6: The schematic model of green sulfur bacterium *chlorobium tepidum* based on [18].

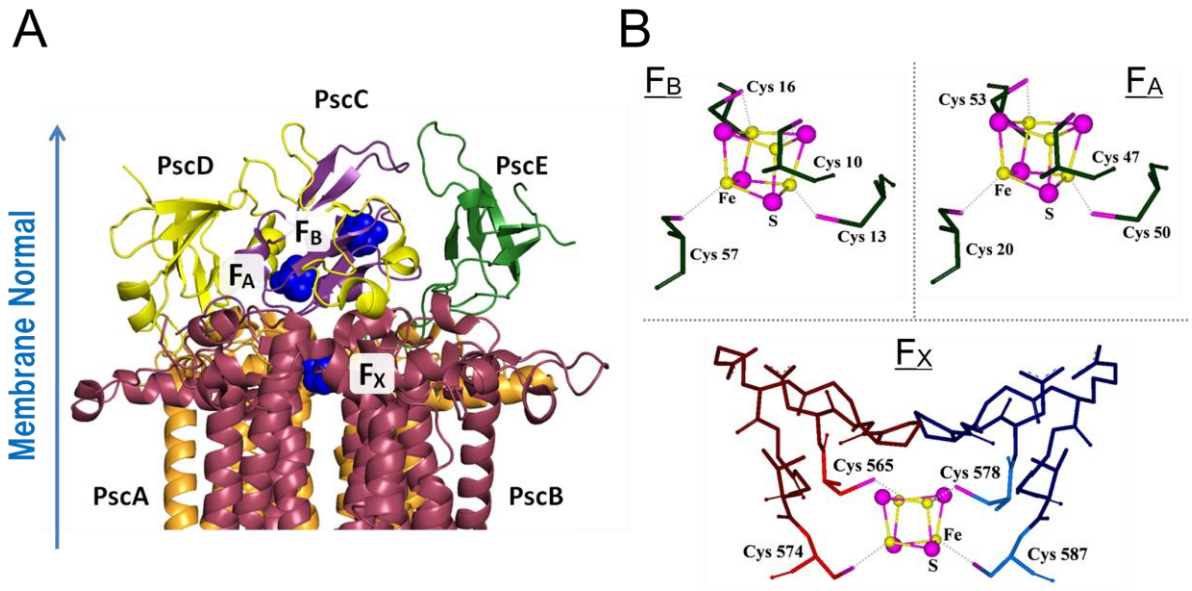

Figure III-7: (A). Protein structure around [4Fe-4S] clusters F_X, F_A, and F_B in PS I RC (PDB entry 1JB0). PsaA, PsaB, PsaC, PsaD, and PsaE subunits are represented in blue, red, purple, green, and yellow, respectively. (B). Binding motifs of the Fe-S clusters which are ligated by four Cys residues. F_X is located between PsaA and PsaB subunits, in which two Cys ligands are provided from each subunit. F_A and F_B are embedded in PsaC subunit. Large spheres in pink and small spheres in yellow represent sulfur (S) and iron (Fe) atoms, respectively. Dotted lines indicate interatomic bonds between Fe atom of the cluster and S atom of Cys residues in protein scaffold.

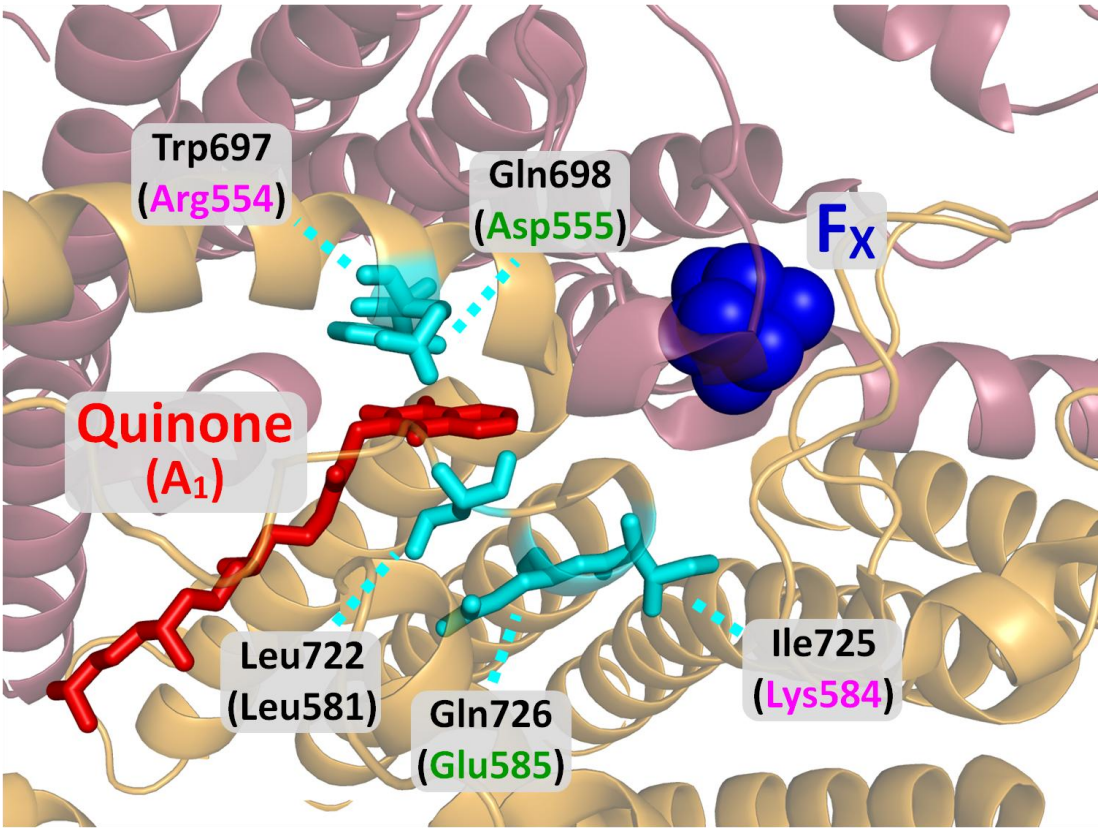

Figure III-8: Structural model of quinone (A_1)-binding site in hRC, which is presumed from the crystal structure of PS I RC [26]. The natural amino acid residues in PS I RC are replaced by charged ones in hRC, shown in blackest. Neutral, positive, and negative amino-acid residues are represented in black, pink, and green, respectively. Leu722 that provides a hydrogen bond to fix a quinone molecule in the binding-site is conserved in hRC.

References

[1] 佐藤 公行, 光合成, 朝倉植物生理学講座 3, （朝倉書店, 東京都, 2002）

[2] Deisenhofer, J., Epp, O., Miki, K., Huber, R. and Michel, H. (1985) Structure of the protein subunits in the photosynthetic reaction center of *Rhodopseudomonas Viridis* at 3Å resolution, Nature 318, 618-624.

[3] Heinent, U., Utschig, L.M., Poluektov, O.G., Link, G., Ohmes, E. and Kothe, G. (2007) Structure of the charge separated state $P_{865}^{+}Q_A^{-}$ in the photosynthetic reaction centers of *Rhodobacter sphaeroides* by quantum beat oscillations and high-field electron paramagnetic resonance: Evidence for light-induced Q_A^{-} reorientation, J. Am. Chem. Soc. 129, 15935-15946.

[4] Calvo, R., Abresch, E.C., Bittl, R., Feher, G., Hofbauer, W., Isaacson, R.A., Lubitz, W., Okamura, M.Y. and Paddock, M.L. (2000) EPR study of the molecular and electronic structure of the semiquinone biradical $Q_A^{\cdot-}Q_B^{\cdot-}$ in photosynthetic reaction centers from *Rhodobacter sphaeroides*, J. Am. Chem. Soc. 122, 7327-7341.

[5] Agalarov, R. and Brettel, K. (2003) Temperature dependence of biphasic forward electron transfer from the phylloquinone(s) A_1 in photosystem I: only the slower phase is activated, Biochim. Biophys. Acta 1604, 7-12.

[6] Olson, J.M. and Blankenship, R.E. (2004) Thinking about the evolution of photosynthesis, Photosynth. Res. 80, 373-386.

[7] Vermaas, W.F.J. (1994) Evolution of heliobacteria: Implications for photosynthetic reaction center complexes, Photosynth. Res. 41, 285-294.

[8] Gest, H. and Favinger, J.L. (1983) *Heliobacterium chlorum*, an anoxygenic brownish green photosynthetic bacterium containing a new form of bacteriochlorophyll, Arch. Microbiol. 136, 11-16.

[9] Madigan, M.T. and Ormerod, J.G. (1995) Taxonomy, physiology and ecology of heliobacteria. In *Anoxygenic Photosynthetic Bacteria* (Blankenship, R.E., Madigan, M.T. and Bauer, C.E., Eds.), pp. 17-30, Kluwer Academic Publishers, Dordrecht, The Netherlands.

[10] Blankenship, R.E. (1992) Origin and early evolution of photosynthesis, Photosynth. Res. 33, 91-111.

[11] Xiong, J., Fischer, W.M., Inoue, K., Nakahara, M. and Bauer, C.E. (2000) Molecular evidence for the early evolution of photosynthesis, Science 289, 1724-1730.

[12] Trost, J.T. and Blankenship, R.E. (1989) Isolation of a photoactive photosynthetic reaction center core antenna complex from *Heliobacillus mobilis*, Biochemistry 28, 9898-9904.

[13] Vandemeent, E.J., Kleinherenbrink, F.A.M. and Amesz, J. (1990) Purification and properties

of an antenna reaction center complex from Heliobacteria, Biochim. Biophys. Acta 1015, 223-230.

[14] Liebl, U., Mockensturmwilson, M., Trost, J.T., Brune, D.C., Blankenship, R.E. and Vermaas, W. (1993) Single core polypeptide in the reaction center of the photosynthetic bacterium *Heliobacillus mobilis*: Structural implications and relations to other photosystems, Proc. Natl. Acad. Sci. USA 90, 7124-7128.

[15] Buttner, M., Xie, D.L., Nelson, H., Pinther, W., Hauska, G. and Nelson, N. (1992) Photosynthetic reaction center genes in green sulfur bacteria and in photosystem 1 are related, Proc. Natl. Acad. Sci. USA 89, 8135-8139.

[16] Vandemeent, E.J., Kobayashi, M., Erkelens, C., Vanveelen, P.A., Amesz, J. and Watanabe, T. (1991) Identification of 8^1-Hydroxychlorophyll *a* as a functional reaction center pigment in heliobacteria, Biochim. Biophys. Acta 1058, 356-362.

[17] Hauska, G., Schoedl, T., Remigy, H. and Tsiotis, G. (2001) The reaction center of green sulfur bacteria, Biochim. Biophys. Acta 1507, 260-277.

[18] Frigaard, N.U., Chew, A.G.M., Li, H., Maresca, J.A. and Bryant, D.A. (2003) *Chlorobium tepidum*: insights into the structure, physiology, and metabolism of a green sulfur bacterium derived from the complete genome sequence, Photosynth. Res. 78, 93-117.

[19] Fromme, P., Jordan, P. and Krauss, N. (2001) Structure of photosystem I, Biochim. Biophys. Acta 1507, 5-31.

[20] Kobayashi, M., Vandemeent, E.J., Erkelens, C., Amesz, J., Ikegami, I. and Watanabe, T. (1991) Bacteriochlorophyll *g* epimer as a possible reaction center component of heliobacteria, Biochim. Biophys. Acta 1057, 89-96.

[21] Rigby, S.E.J., Evans, M.C.W. and Heathcote, P. (2001) Electron nuclear double resonance (ENDOR) spectroscopy of radicals in photosystem I and related Type 1 photosynthetic reaction centres, Biochim. Biophys. Acta 1507, 247-259.

[22] Mizoguchi, T., Oh-oka, H. and Tamiaki, H. (2005) Determination of stereochemistry of bacteriochlorophyll g_F and 8^1-hydroxy-chlorophyll a_F from *Heliobacterium modesticaldum*, Photochem. Photobiol. 81, 666-673.

[23] Heinnickel, M., Shen, G.Z. and Golbeck, J.H. (2007) Identification and characterization of PshB, the dicluster ferredoxin that harbors the terminal electron acceptors F_A and F_B in *Heliobacterium modesticaldum*, Biochemistry 46, 2530-2536.

[24] Oh-oka, H. (2007) Type 1 reaction center of photosynthetic heliobacteria, Photochem. Photobiol. 83, 177-186.

[25] Heinnickel, M. and Golbeck, J.H. (2007) Heliobacterial photosynthesis, Photosynth. Res. 92, 35-53.

[26] Miyamoto, R., Iwaki, M., Mino, H., Harada, J., Itoh, S. and Oh-oka, H. (2006) ESR signal of the iron-sulfur center F_X and its function in the homodimeric reaction center of *Heliobacterium modesticaldum*, Biochemistry 45, 6306-6316.

[27] Kleinherenbrink, F.A.M., Chiou, H.C., Lobrutto, R. and Blankenship, R.E. (1994) Spectroscopic evidence for the presence of an iron sulfur center similar to F_X of photosystem I in *Heliobacillus mobili*s, Photosynth. Res. 41, 115-123.

[28] Heinnickel, M., Agalarov, R., Svensen, N., Krebs, C. and Golbeck, J.H. (2006) Identification of F_X in the heliobacterial reaction center as a [4Fe-4S] cluster with an S = 3/2 ground spin state, Biochemistry 45, 6756-6764.

[29] Baymann, D., Brugna, M., Muhlenhoff, U. and Nitschke, W. (2001) Daddy, where did (PS)I come from?, Biochim. Biophys. Acta 1507, 291-310.

[30] Lin, S., Chiou, H.C. and Blankenship, R.E. (1995) Secondary electron transfer processes in membranes of *Heliobacillus mobilis*, Biochemistry 34, 12761-12767.

[31] Nuijs, A.M., Vandorssen, R.J., Duysens, L.N.M. and Amesz, J. (1985) Excited states and primary photochemical reactions in the photosynthetic bacterium *Heliobacterium chlorum*, Proc. Natl. Acad. Sci. USA 82, 6865-6868.

[32] Nuijs, A.M., Vasmel, H., Joppe, H.L.P., Duysens, L.N.M. and Amesz, J. (1985) Excited states and primary charge separation in the pigment system of the green photosynthetic bacterium *Prosthecochloris aestuarii* as studied by picosecond absorbance difference spectroscopy, Biochim. Biophys. Acta. 807, 24-34.

[33] Hastings, G., Kleinherenbrink, F.A.M., Lin, S., Mchugh, T.J. and Blankenship, R.E. (1994) Observation of the reduction and reoxidation of the primary electron acceptor in photosystem I, Biochemistry 33, 3193-3200.

[34] Kumazaki, S., Iwaki, M., Ikegami, I., Kandori, H., Yoshihara, K. and Itoh, S. (1994) Rates of primary electron transfer reactions in the photosystem I reaction center reconstituted with different quinones as the secondary acceptor, J. Phys. Chem 98, 11220-11225.

[35] van der Est, A., Hager-Braun, C., Leibl, W., Hauska, G. and Stehlik, D. (1998) Transient electron paramagnetic resonance spectroscopy on green-sulfur bacteria and heliobacteria at two microwave frequencies, Biochim. Biophys. Acta 1409, 87-98.

[36] Brettel, K., Leibl, W. and Liebl, U. (1998) Electron transfer in the heliobacterial reaction center: evidence against a quinone-type electron acceptor functioning analogous to A_1 in photosystem I, Biochim. Biophys. Acta 1363, 175-181.

[37] Kleinherenbrink, F.A.M., Ikegami, I., Hiraishi, A., Otte, S.C.M. and Amesz, J. (1993) Electron transfer in menaquinone depleted membranes of *Heliobacterium chlorum*, Biochim. Biophys. Acta 1142, 69-73.

[38] Brok, M., Vasmel, H., Horikx, J.T.G. and Hoff, A.J. (1986) Electron transport components of *Heliobacterium chlorum* investigated by EPR Spectroscopy at 9 and 35 GHz, FEBS Lett. 194, 322-326.

[39] Muhiuddin, I.P., Rigby, S.E.J., Evans, M.C.W., Amesz, J. and Heathcote, P. (1999) ENDOR and special TRIPLE resonance spectroscopy of photoaccumulated semiquinone electron acceptors in the reaction centers of green sulfur bacteria and heliobacteria, Biochemistry 38, 7159-7167.

[40] Nitschke, W., Setif, P., Liebl, U., Feiler, U. and Rutherford, A.W. (1990) Reaction center photochemistry of *Heliobacterium chlorum*, Biochemistry 29, 11079-11088.

[41] Trost, J.T., Brune, D.C. and Blankenship, R.E. (1992) Protein sequences and redox titrations indicate that the electron acceptors in reaction centers from heliobacteria are similar to photosystem I, Photosynth. Res. 32, 11-22.

[42] van der Est, A. (2001) Light-induced spin polarization in type I photosynthetic reaction centres, Biochim. Biophys. Acta 1507, 212-225.

[43] 日本光合成研究会，光合成事典，（学会出版センター，東京都, 2003）

[44] Antonkine, M.L., Jordan, P., Fromme, P., Krauss, N., Golbeck, J.H. and Stehlik, D. (2003) Assembly of protein subunits within the stromal ridge of photosystem I. Structural changes between unbound and sequentially PSI-bound polypeptides and correlated changes of the magnetic properties of the terminal iron sulfur clusters, J. Mol. Biol. 327, 671-697.

Orientations of Iron Sulfur Clusters in Homodimeric Type I Photosynthetic Reaction Center of *Heliobacterium modesticaldum*

Introduction

Heliobacteria are strict anaerobes discovered in 1983 [1] and form a Gram-positive bacterial group that is exceptional in the photosynthetic bacterial clade [2]. Heliobacteria use bacteriochlorophyll (BChl) *g* that absorbs at around 800 nm as the major photosynthetic pigment [3]. The structure and absorption spectrum of BChl *g* are closer to those of BChl *a* or *b*, used in all the other photosynthetic bacteria, whereas BChl *g* is readily oxidized in aerobic condition to structurally and spectroscopically Chl *a*-like molecule as used in plants and cyanobacteria, which absorbs the light at the shorter wavelengths. Heliobacteria contains Type I reaction center (RC), designated hRC hereafter, that is a simplest photosynthetic system with no light-harvesting antenna complex [4] in contrast to all the other RCs of photosynthetic bacteria and plants [3,5-9]. The hRC is made of two identical PshA subunits that form a so-called "homodimer RC" [10-12] and contains 35-40 BChl *g* molecules that function as the antenna pigments and the electron donor [4]. A homodimeric structure is also found in green sulfur bacterial RC (gRC) that consists of two PscA subunits [5]. The structures of the homodimer RCs have not been resolved yet, whereas the x-ray crystallographic structure of a heterodimeric RC of photosystem I (PS I) that consists of PsaA and PsaB subunits has been available [13,14]. The homology of amino acid sequence of PshA subunit to PscA subunit of gRC, and PsaA or PsaB subunit of PS I, is low but still indicates the common structural feature among these Type I RCs [2,12]. It is also suggested that both the homodimer and heterodimer RCs are assumed to be evolved from a common ancestral homodimer RC [6,7]. It is, therefore, interesting how Type I RCs varied in the course of evolution from the hRC-type (or gRC-type) homodimer to PS I-type heterodimer. However, information for the structure and the electron transfer system in hRC has been scarce. In this study, we first characterized orientations of iron sulfur clusters that work as terminal electron acceptors in hRC.

Electron transfer pathway in hRC can be assumed to contain five (or six) types of cofactors, P800, A_0, (A_1), F_X, and F_A/F_B in analogy to PS I [8,9]. The primary electron donor P800 is identified as a special pair of BChl *g* (or a heterodimer of BChl *g* and *g'*) as a counterpart of a special pair of Chl *a* (P700) in PS I [15,16]. The primary electron acceptor A_0 is a derivative of chlorophyll *a*,

8^1-hydroxy-Chl *a* (8^1-OH-Chl *a*) [4,17]. This resembles A_0 in PS I that is a monomeric Chl *a* ligated by methionine residue in PS I. Menaquinone-9 molecules, which are contained in hRC [10], may function as the secondary electron acceptor A_1 analogous to phylloquinone (A_1) in PS I. However, the evidence for the function of A_1 has been scarce or even negative [18-21], except for the detection of a flash-induced transient electron spin polarized (ESP) signal that was proposed to arise from the $P800^+A_1^-$ radical pair [22].

F_A and F_B are contained in hRC as the two [4Fe-4S] type clusters on the PshB subunit bound to hRC [23]. PshB is assumed to be a counterpart of PsaC bound to PS I, or PscB bound to gRC [23], although the similarities among the amino acid sequences of these polypeptides are rather low each other. The redox potential of F_B is assumed to be more positive than that of F_A because of its preferential photo-accumulation at cryogenic temperature [24]. The situation in hRC, however, is inconsistent with that in PS I, where the redox potential of F_B is lower than that of F_A [25]. Thus the characteristics of F_A and F_B in hRC have not been clear, preventing from understanding of the electron transfer in the reducing side of hRC.

As for F_X in hRC, no EPR signal has been detected for a long time [24,26-28], although the small absorption changes at around 430 nm detected in the urea-treated membranes were considered to be derived from F_X^- [28]. In analogy to PS I, F_X is assumed to be located at the top center of hRC at the interface between the two PshA subunits [12] based on the homology of ligands on RC polypeptides [29]. Miyamoto *et al*. (2006) detected a light-induced transient EPR signal with g_z = 2.040, g_y = 1.911, and g_x = 1.896 and assigned it to F_X^- in the membranes of *Hbt. modesticaldum* that were frozen in the presence of dithionite. This "$S_{1/2}$ F_X signal*"* was detected only transiently during the illumination even at 5 K, and decayed in parallel with $P800^+$ with a time constant of less than 10 ms after the flash excitation. On the other hand, Heinnickel *et al*. (2006) photo-accumulated an EPR signal at g = 5 and 2 regions, and assigned it to arise from "$S_{3/2}$ F_X signal*"* in membrane and hRC core preparations from the same species. The signal was stable in the dark even after illumination. The two groups, therefore, identified F_X^- with different spin states and kinetic behaviors in hRC. The property and function of F_X in hRC, thus, remains to be studied in more detail.

All the type I RCs contain three FeS clusters. However, the currently available information in hRC is not sufficient to fully characterize the three FeS clusters. We, therefore, studied the orientations of FeS cluster EPR signals in the oriented membranes of *Hbt. modesticaldum* because the orientations of the principal axes in the g-tensor of the FeS clusters are known to clearly characterize the properties of F_A, F_B, and F_X clusters in PS I [30-34] and in gRC [35]. The orientation of F_B^- in hRC measured in this study was very similar to that of F_A^- in PS I, and that of "$S_{1/2}$ F_X^-" signal was comparable to that of F_X^- in PS I.

Materials and methods

Sample preparations

A strain of Hbt. modesticaldum was generously provided by M. T. Madigan (Southern Illinois University, Carbondale, IL). Cells were grown anaerobically in a PYE medium in a 1 L bottle under continuous illumination with tungsten lamps [36]. To avoid the accumulation of an appreciable amount of lysed cells in the late-logarithmic growth phase, cultivation was performed at 47 °C for 18-20 h using 1% inocula [37].

All the procedures for the preparations of membranes as well as the EPR measurements were carried out under anaerobic conditions, as previously described [38]. All the media were fully degassed and flushed with N_2 gas before being used.

The cells were harvested by centrifugation at 12,000g for 10 min, suspended in 7-8 mL of buffer A [50 mM Tris-HCl (pH 8.0), 1 mM EDTA, and 2 mM DTT], and disrupted by being passed through a French pressure cell three times at 20,000 psi. After removal of the cell debris by centrifugation at 12,000 g for 10 min, the membranes were collected by ultracentrifugation at 180,000 g for 1 h, and suspended in buffer B that contained 200 mM glycine-KOH (pH 10.0), 1 mM EDTA, and 2 mM DTT. After ultracentrifugations, the membranes obtained were directly pasted on thin polyester sheets to prepare oriented membranes (see below). Membrane fragments of spinach PS I were prepared as described in [39].

Orientations of membranes

Oriented membrane multi-layers were prepared as described by Mino et al. [40]. The membranes isolated from Hbt. modesticaldum were spread on thin polyester sheets. The sheets were then dried in the dark for 5-7 hours at 4 ^{o}C by flushing with N_2 gas that was supplied through the buffer containing dithionite. Several strips of the sheets were layered in parallel in an EPR tube and frozen in the dark. In the measurements, the layers of sheets in the tube were set to be perpendicular to the external magnetic field. Signals were measured by rotating layers at each 15^{o} between the membrane normal and the external magnetic field. It was difficult to set the sheets completely parallel to the external magnetic field so that we estimated the accurate orientation angle of the membranes from the polar plotting of signal intensities of Rieske-FeS center, which can be assumed to give an accurate direction in parallel to the membrane normal. A similar method was used for the preparation and measurements of the oriented membrane fragments of spinach PS I.

EPR measurements

EPR measurements were carried out using a Bruker ESP-300E X-band spectrometer with 100 kHz field modulation (Bruker Biospin, Germany) equipped with a liquid-helium flow cryostat and a temperature control system (CF935, Oxford Instruments, Oxford, UK). Continuous white light illumination was given from a 500 W tungsten lamp through heat-cut glass filters. No heating effect under illumination was checked by monitoring the intensity of EPR signal of tyrosine D radical in photosystem II (data not shown).

Results

EPR spectra of Rieske-type FeS cluster and F_B in oriented membranes of Hbt. modesticaldum

Figure 1A shows derivative type EPR spectra measured in the dark at 14 K in the oriented membranes of *Hbt. modesticaldum* frozen in the presence of 2 mM DTT, in which angles indicate those between the membrane normal and the external magnetic field. The oriented membranes were rotated in the external field. The spectra showed strong angular dependency. The peaks at g = 2.038 and 1.822 can be assigned to g_z and g_x peaks of a Rieske FeS cluster, respectively, as previously assigned based on the redox titration [41]. The intensities at these two g-values were plotted against angles (polar plots) in Fig. 1B *a* and *b*, respectively. The g_z intensities were evaluated carefully by analyzing the third derivative spectra too. The peak intensities at g_z and g_x showed maxima at 90^o and 0^o, respectively, in consistent with the previous report [41]. The result indicated that the membranes of *Hbt. modesticaldum* were well oriented under the present experimental conditions. Therefore, we used these peaks as the conventional marker of orientation of membranes and defined the angles that gave maximal peak intensities at g_z and g_x in the Rieske FeS cluster as 90^o and 0^o, respectively, in the following measurements. The g_y peaks were somewhat ambiguous due to the overlap of other signals such as F_B^-, which was reduced partially by DTT under the present high-pH condition.

Under the same conditions, EPR spectra induced by the illumination at 14 K were measured at an angle of 63^o between the membrane normal and the external magnetic field in the same oriented membranes (Fig. 2A). Traces *a* in Fig. 2A show the spectra measured before (broken line) and during illumination (solid line). Trace *b* shows a light-minus-dark difference spectrum, which was calculated as the solid line–minus-broken line in *a*. The difference spectrum was characterized by g-values of g_z = 2.066, g_y = 1.937, and g_x = 1.890. The measured g-values were almost the same as those of g_z = 2.069, g_y = 1.938, and g_x = 1.891 of the F_B^- signal reported previously in the ”unoriented” membranes of *Hbt. modesticaldum* [37]. To avoid the partial decay of F_B^- due to its recombination with $P800^+$ during the time-consuming measurement, the light-minus-dark difference spectrum was calculated as the difference between the spectra measured before and during the continuous illumination.

Similar light-minus-dark difference spectra were calculated from the sets of light and dark spectra measured at each 15^o (Fig. 2B). The signal intensities at g_z = 2.066, g_y = 1.937, and g_x = 1.890 were polar-plotted in Fig. 3A *a*, *b*, and *c*, respectively. The g_y intensities of each spectrum were evaluated by calculating the second derivative spectrum. The peak intensities at g_z, g_y, and g_x showed maxima at 60^o, 60^o, and 45^o, respectively. The spectra in Fig. 2B also showed slight positive

and negative peaks at g = 2.036 and 1.820 of Rieske FeS cluster signal, which exhibited maxima at 90^o and 0^o, respectively, as seen in Fig. 1.

Measurements were also done in the oriented membranes of spinach PS I that was frozen in the dark with 20 mM ascorbate. After 20 min illumination at 14 K, EPR spectra were measured in the dark at each 15^o (Fig. 2C). The peaks at g_z = 2.050, g_y = 1.947, and g_x = 1.871 were attributed to F_A^-, and those at g_z = 2.068, g_y = 1.933, and g_x = 1.891 to F_B^-. The peaks at g_z, g_y and g_x showed maxima at 65^o, 50^o and 50^o for F_A (Fig. 3B *a-c*), and 30^o, 60^o and 90^o for F_B (Fig. 3B *d-f*), respectively, in the polar plots. The orientations were consistent with those reported previously in PS I of spinach [30], *Dunaliella parva* [31], *Synechocystis* sp. PCC6803 [32], and *Synechococcus elongatus* [33] (see Table I). It is, therefore, concluded that the orientation of F_B on the PshB protein in *Hbt. modesticaldum* membrane is similar to that of F_A in PS I, and is different from that of F_B in PS I.

Angular dependence of light-induced EPR signal of FeS cluster

The oriented membranes of *Hbt. modesticaldum* were soaked in 200 mM glycine-KOH buffer (pH 10.0) containing 60% (v/v) glycerol and an excess amount of dithionite, and incubated in the dark at room temperature for 5 min to chemically reduce F_A and F_B. The sample was then cooled down to 5 K in the dark (the freezing in the presence of 60% glycerol produced the clear frozen sample with low light scattering and low distortion of oriented membranes). Figure 4A shows the effect of illumination at 5 K on the EPR spectrum of the oriented membranes placed at 7^o between the membrane normal and the external magnetic field. Solid and broken lines (in traces *a*) show the spectra measured under illumination and in the dark after illumination, respectively. The light-minus-dark difference spectrum (trace *b*) was characterized by g-values of g_z = 2.046, g_y = 1.915, and g_x = 1.905. The g-values and spectral shape of the signal are obviously different from those of F_B^-, and are closer to those of the light-induced "$S_{1/2}$ type F_X" signal reported in the "unoriented" membranes of *Hbt. modesticaldum* [37]. We could not detect the "$S_{3/2}$ F_X^- signal" in the g = 2-5 region, reported by Heinnickel et al. (2006), under the present experimental conditions, both during illumination at cryogenic temperature and after pre-illumination at 210 K followed by cooling in the light. Therefore, we measured the orientation of the "$S_{1/2}$ type signal" carefully.

Figure 4B shows the light-minus-dark difference spectra measured at various angles. The signal intensities at g_z = 2.046 and g_y = 1.915 were polar-plotted in Fig. 5A. The g_y intensities were evaluated by calculating the second derivative spectra to minimize the contribution of g_x peak. The intensities of g_z and g_y peaks became maximal at 0^o and 90^o, respectively. The direction of the cosine of the axes of the principal g-tensor is expressed by the following equation:

$$\sum_{i=x,y,z} \cos^2 \theta_i = 1 \qquad \text{(Eq.1)},$$

where θ_i is an angle of the g_i axis between membrane normal and the external magnetic field. Therefore, an angle of the g_x axis was estimated to be at 90^o from the membrane normal.

The angular dependent spectra also showed slight positive peaks at g = 2.068 and 2.038 and negative peaks at 1.939 and 1.821. The peaks were maximum at 60^o, 90^o, 60^o, and 0^o, respectively (polar plots are not shown). The peaks at g = 2.068 and 1.939 could be attributed to a portion of F_B^-, as seen in Fig. 2, and the other two peaks to the Rieske FeS cluster, as seen in Fig. 1, on the basis of their g-values and angular dependencies.

We also prepared the oriented membranes of spinach PS I in a medium containing 200 mM glycine-KOH buffer (pH 10.0), 60% (v/v) glycerol, and an excess amount of dithionite. After the dark incubation at room temperature for 5 min, the sample was illuminated for 1 hour at 210 K and then cooled down to 5 K under illumination to accumulate F_X^-, followed by the angular dependent EPR measurement in the dark at 14 K as shown in Figure 4C. The peaks at g = 2.12-1.85 were mainly attributed to the spin-interacting state of F_A^-/F_B^- and partially to the g_z and g_y peaks of F_X^-, which also gave the g_x peak at 1.773. The g_z and g_y peaks of F_X^- were ambiguous due to the overlap of the interacting F_A^-/F_B^- signal. The peak intensity at g_x = 1.773 of F_X^- was maximal at 0^o as polar-plotted in Fig. 5B. Based on Eq. 1, the angles of the g_z and g_y axes could be estimated to be 90^o from the membrane normal. The orientations of the principal axes in the g-tensor of F_X were thus consistent with those reported in spinach PS I [34], *Dunaliella parva* [31], and *Synechocystis* 6803 [32] as listed in Table I.

Discussion

Orientation of F_B^- in hRC

Table I shows the g-values and orientations of the principal axes in the g-tensor of FeS clusters in hRC, determined in this study, with those reported in gRC [35] and PS I RC [30-32]. The orientations of F_A and F_B clusters in PS I are fairly conserved in a wide range of cyanobacteria, green algae, and plants, probably because of the high similarity of amino acid sequences of their PsaC subunits. The orientations in the g-tensor of F_B in gRC also appear to be similar. However, Table I indicates that the orientation of principal axes of F_B in hRC is different from those of F_B in gRC or PS I, and rather closer to those of F_A. Figure 6A and B show schematic models of the g-tensor orientation of FeS clusters in (A) hRC and (B) PS I.

EPR signal of a FeS cluster was reported first in membranes of *Hbt. chlorum* [26]. The signal, which was accumulated after illumination at 5 K in the presence of ascorbate, was characterized with g-values of $g_z = 2.07$, $g_y = 1.93$, and $g_x = 1.89$, and named F_B^- because the g-values resemble those of the F_B^- signal in PS I [24]. The redox potentials of F_A and F_B clusters were estimated to be about -440 to -510 mV, respectively, by the indirect measurement based on the $P800^+$ decay kinetics [26,27] or around -600 mV based on the photoreduction behavior in the chemically pre-reduced membranes [24]. The preferential photo-accumulation of F_B^- at 5 K in hRC suggested its redox potential to be more positive than F_A and F_X [24], as was the case for F_B in gRC [35]. The situation of F_B^- in hRC and gRC, however, are different from the situation in PS I because the redox potentials of F_A and F_B in PS I are estimated to be -550 and -585 mV, respectively [25]. Thus, the redox property of F_B in hRC and gRC is somewhat different from that of F_B in PS I, although they show similar g-values.

In heliobacterial membranes, the illumination at 200 K in the presence of dithionite induced the spin-interacting signal of F_A^-/F_B^- [24] with $g_z = 2.05$, $g_y = 1.95$, and $g_x = 1.90$, although the orientation of this state could not be studied in the oriented membranes produced in the present study. Similar magnetic interactions between the F_A and F_B clusters were also reported in gRC (Nitschke et al. 1990b) and in PS I [42]. The F_A and F_B clusters are known to exist in the 8 kDa PshB protein in hRC [23,43], and in the 24 kDa PscB protein in gRC [5]. The amino acid sequence of PshB contains two typical CxxCxxCxxxCP motifs for the [4Fe-4S] clusters as PsaC does [23], while that of PscB contains one with this type together with a modified motif of CxxCxxCxxxxxCP [5]. These proteins show rather low homologies each other. The different orientations of F_B in different Type I RCs, thus, might reflect different protein structures. Another idea is that the nomenclatures of these clusters done with respect to their g-values are not adequate as discussed in the section of electron transfer below.

Orientation of the F_X-type cluster

We determined the g-values and orientation of the EPR signal induced by the illumination at 5 K in the oriented membranes of *Hbt. modesticaldum* in the presence of dithionite. This signal, which was completely different from the F_B^- one, could be assigned to either F_A^- or F_X^-. The orientations of g_z, g_y, and g_x axes in the g-tensor of the 5 K-light-induced signal were characterized by angles of 0^o, 90^o, and 90^o, which were more similar to 90^o, 90^o, and 0^o for F_X^- in PS I compared to 65^o, 50^o, and 50^o for F_A^- in PS I. As reported previously, this type of light-induced EPR signal was detected in the "unoriented" membranes under the same conditions [37]. The rapid spin relaxation rate of this signal, estimated by its detection at the high microwave power at very low temperatures, resembles that of F_X in PS I [37,44]. The amplitude of this signal is known to decay with a time constant of less than 10 ms, which is comparable to the decay time constant of the flash-induced $P800^+$ signal [37] or to the 1.0-4.5 ms decay time constant of the spin-polarized $P800^+F_X^-$ state reported in the membranes of *Hba. mobilis* [20]. Therefore, we have assigned the 5 K-light-induced signal detected in the orientated membranes to correspond to "$S_{1/2}$ F_X^-" signal as previously done by Miyamoto et al (2006). We could not detect the "$S_{3/2}$ F_X^- signal" measured in similar hRC preparations by Heinnickel et al. (2006) in this study. In this study, thus, we discussed the g-values and orientation of the "$S_{1/2}$-type signal", although further studies on both the "$S_{1/2}$" and "$S_{3/2}$" F_X^- signals are required to solve the controversy.

Structure of F_X in hRC

Figure 6C shows the binding motif of F_X cluster in PS I, in which four Fe atoms of F_X are ligated by four cystein residues, two from PsaA and the other two from PsaB subunit. The electronic structure of F_X^- is, thus, expected to be affected by the heterogeneous coordination. On the other hand, we can expect heliobacterial F_X to be ligated by two identical PshA subunits. Table I indicates differences in the g-values and orientations of F_X^- between hRC and other Type I RCs despite the high similarity among the amino acid sequences of RC proteins around their F_X-binding sites. First, the axis parallel to the membrane normal was the g_z axis for heliobacterial "$S_{1/2}$ F_X", while it is the g_x axis for F_X of PS I or gRC. Second, the "$S_{1/2}$ F_X^-" signal with g-values of $g_z = 2.046$, $g_y = 1.915$, and $g_x = 1.905$ in hRC suggests axial symmetry higher than that of PS I ($g_z = 2.08$, $g_y = 1.88$, and $g_x = 1.78$) [45] or of gRC ($g_z = 2.17$, $g_y = 1.92$, and $g_x = 1.77$) [46].

Each F_X^- signal shows a little different isotropic g-value (g_{iso}), which can be calculated as an average of the g_z, g_y, and g_x values to be 1.955 for hRC, 1.91 for PS I, and 1.95 for gRC. The difference (Δg) between the g_{iso} and the g-values along the membrane normal is 0.091 for hRC, 0.13 for PS I, and 0.18 for gRC. The small Δg in hRC suggests the smaller structural distortion of F_X along the membrane normal. The plane along the membrane surface includes the g_x and g_y axes in hRC, and the g_y and g_z axes in PS I and gRC. The differences between the two g-values within this

plane were calculated to be 0.01 for hRC, 0.2 for PS I, and 0.25 for gRC. Therefore, F_X structure in hRC is more symmetric along the membrane surface compared to those in PS I and gRC. The results suggest that the "$S_{1/2}$ F_X cluster" in hRC has symmetry higher than that in the heterodimeric PS I or the homodimeric gRC. The asymmetry in the homodimeric gRC might be induced by the bindings of some more peripheral proteins on the F_X side in addition to PscB (F_A/F_B protein), such as PscD (a 17-18 kDa polypeptide), and extra FMO proteins (light-harvesting trimeric pigment-protein complex) linked to the large chlorosomes [47]. F_X in hRC, which binds only a small PshB (F_A/F_B protein), therefore, seems to retain the high symmetry in the homodimer structure.

Electron transfer through FeS clusters in hRC

The forward electron transfer in the reducing side of PS I is known to occur as $A_1 \rightarrow F_X \rightarrow F_A \rightarrow F_B$ [48]. The $A_1 \rightarrow F_X \rightarrow F_A$ process is a downhill energy process, while the subsequent $F_A \rightarrow F_B$ step is an uphill process because the redox potential of F_A is more positive than that of F_B [25]. In hRC, function of A_1 (menaquinone) has been questioned by negative circumstantial evidences [8,9] except for the two studies; the photoaccumulation of semiquinone [49,50] and the detection of the ESP-EPR signal, which was proposed to originate from the $P800^+A_1^-$ state [22]. Therefore, the function of A_1 is not clear yet in hRC at present. In the study, we confirmed that F_B^- in hRC was preferentially photo-accumulated in agreement with its more positive redox potential compared to that of F_A [24]. It indicates that F_B in hRC behaves like F_A in PS I as for the redox potential. The result in this study also indicated that the orientation of F_B^- in hRC resembles that of F_A^- in PS I. Therefore, if the electron transfer in hRC occurs as $F_X \rightarrow F_B \rightarrow F_A$, then the whole process becomes a combination of downhill and uphill processes as that in PS I. In that case, F_A and F_B in hRC are assumed to function as F_B and F_A in PS I, respectively (Fig. 6B), and names of F_A and F_B in hRC would be better to be exchanged each other to correspond with the situation in PS I. The situation assumed in hRC might be somewhat different in gRC, and another possibility still remains that the electron transfer in hRC occurs very differently from that in PS I.

The "$S_{1/2}$ F_X^-" signal was detected during illumination even at 5 K, which is somewhat different from the situation in PS I, where the flash-induced reduction of F_X is almost suppressed below 200 K due to the suppression of the electron transfer from A_1 to F_X [51]. It is also known that the charge recombination reaction between F_X^- and $P700^+$ in PS I occurs very slowly with a time constant of 130 ms at 5 K [52]. In hRC, the "$S_{1/2}$ F_X^-" signal decays rapidly with a time constant of less than 10 ms even at 5 K, indicating its fast charge recombination [37]. These properties of F_X in hRC are in contrast to the situation in PS I. The mechanism of almost activation-less response of the "$S_{1/2}$ F_X^-" signal remains to be studied.

Conclusion

We assume that the 5K-light-induced EPR signal to originate from "$S_{1/2}$ F_X" based on the orientation of principal *g*-axes, and that F_X in hRC has a structure more symmetrical than F_X in the other Type I RCs. Though, more works are required to solve the controversy between the $S_{1/2}$ and $S_{3/2}$ type signals of F_X in hRC. Redox property of the "$S_{1/2}$ F_X" in hRC seems to be comparable to that in PS I or in gRC, because the signal could be detected only at the extremely reducing conditions. The F_B cluster in PshB protein of hRC was shown to have an orientation and redox property similar to F_A rather than F_B in PS I. Therefore, we assumed F_B in hRC to be an immediate electron acceptor for F_X as F_A does in PS I. F_X showed fast flash-induced reduction and re-oxidation in hRC. This is different from the situation in PS I, in which the reduction and re-oxidation of F_X are significantly suppressed below 200 K. The similarity and difference in characteristics of the cofactors and reactions in hRC still remain to be solved at present. It must be important to understand the evolution of Type I RCs.

Tables

type of RC		homodimeric type I RC		heterodimeric PS I RC			
strain name		Heliobacteria *Hbt.modesticaldum* (this work)	green sulfur bacteria *Chlorobium limicola* (Ref. 35)	plants Spinach (left: this work , right: Ref. 30)		green algae *Dunaliella parva* (Ref. 31)	cyanobacteria *Synechocystis* 6803 (Ref. 32)
F_A/F_B binding protein		PshB	PscB	PsaC			
F_A	g_z	----	----	2.050 (65° ± 5°)	2.05 (65°)	2.053 (65°)	2.050 (65°)
	g_y	----	1.94 (35°)	1.947 (50° ± 5°)	1.94 (50°)	1.94 (55°)	1.942 (48°)
	g_x	----	----	1.871 (50° ± 5°)	1.86 (50°)	1.844 (45°)	1.855 (52°)
F_B	g_z	2.066 (60° ± 5°)	2.07 (30-40°)	2.068 (30° ± 5°)	2.07 (40°)	2.072 (35°)	2.067 (30°)
	g_y	1.937 (60° ± 5°)	1.91 (50°)	1.933 (60° ± 5°)	----	1.92 (55°)	1.92 (60°)
	g_x	1.890 (45° ± 5°)	1.86 (90°)	1.891 (90° ± 5°)	----	1.876 (90°)	1.886 (90°)
F_X binding protein		PshA / PshA	PscA / PscA	PsaA / PsaB			
F_X	g_z	2.046 (0° ± 5°)	---- (90°)*	---- (90°)*	---- (90°)*	---- (90°)*	---- (90°)*
	g_y	1.915 (90° ± 5°)	---- (90°)*	---- (90°)*	---- (90°)*	---- (90°)*	---- (90°)*
	g_x	1.905 (90° ± 5°)*	1.78 (0°)	1.773 (0° ± 5°)	1.78 (0°)[a]	1.745 (0°)	1.755 (0°)

* : deduced from Equation 1
a : See Ref. 34

Table I: g-values and orientations of g-tensor of FeS clusters in Type I RCs of heliobacteria, green sulfur bacteria, and PS I.

Figures

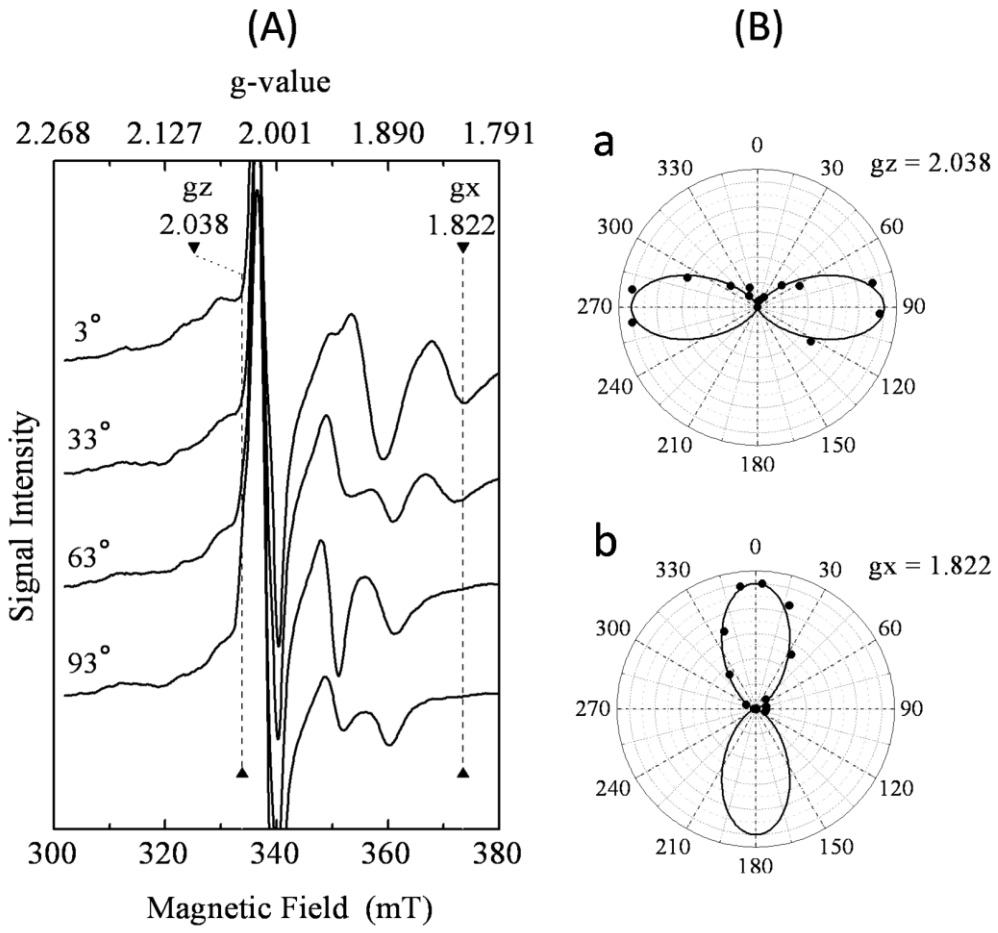

Figure 1: (A): Angular-dependence of an EPR spectrum of the oriented membranes of *Hbt. modesticaldum* frozen in the dark in the presence of 2 mM DTT. Peak positions of the signal of Rieske FeS center are indicated by triangles together with the g-values. Angles between the membrane normal and the external magnetic field are indicated in the figure. (B): Polar plots of the intensities at (a) g_z and (b) g_x peaks of the Rieske FeS center signal indicated in (A). θ (^{o}) refers to the angle between the membrane normal and the external magnetic field. Experimental conditions for the measurements: temperature, 14 K; microwave power, 10 mW; microwave frequency, 9.525 GHz; modulation amplitude, 20 G at 100 KHz; time constant, 20 ms.

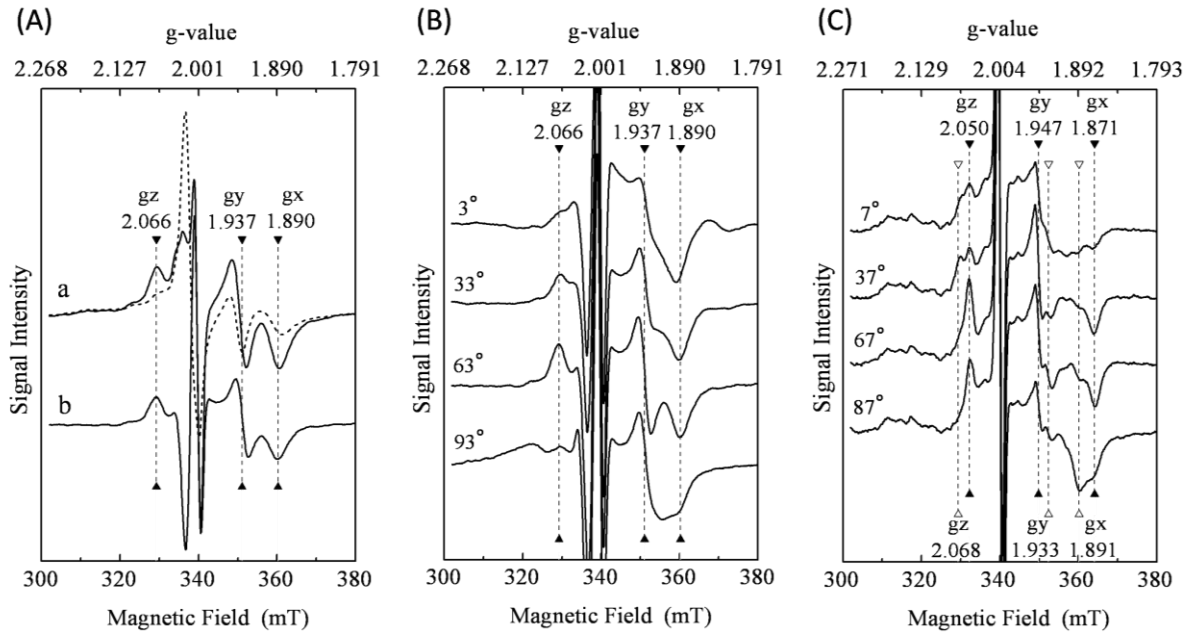

Figure 2: (A): EPR spectra of oriented membranes of *Hbt. modesticaldum* in the presence of 2 mM DTT measured at an angle of 63^{o} between the membrane normal and the external magnetic field. (a) Measured in the dark before and during illumination (broken and solid lines), respectively, at 14 K. (b) Light-minus-dark difference spectrum calculated from the two spectra in (a). Peak positions are indicated by triangles together with the g-values. (B): Light-minus-dark difference spectra at different angles. Samples and experimental conditions were the same as in (A). (C): Angular dependence of EPR spectra of the oriented membranes of spinach PS I frozen in the presence of 20 mM ascorbate. Signals were measured in the dark after 20 min illumination at 14 K. Filled and open triangles indicate the peak positions of F_A^- and F_B^- signals at indicated *g*-values, respectively. Experimental conditions for the measurements: temperature, 14 K; microwave power, 10 mW; microwave frequency, 9.525 GHz (A and B) and 9.535 GHz (C); modulation amplitude, 20 G at 100 KHz; time constant, 20 ms.

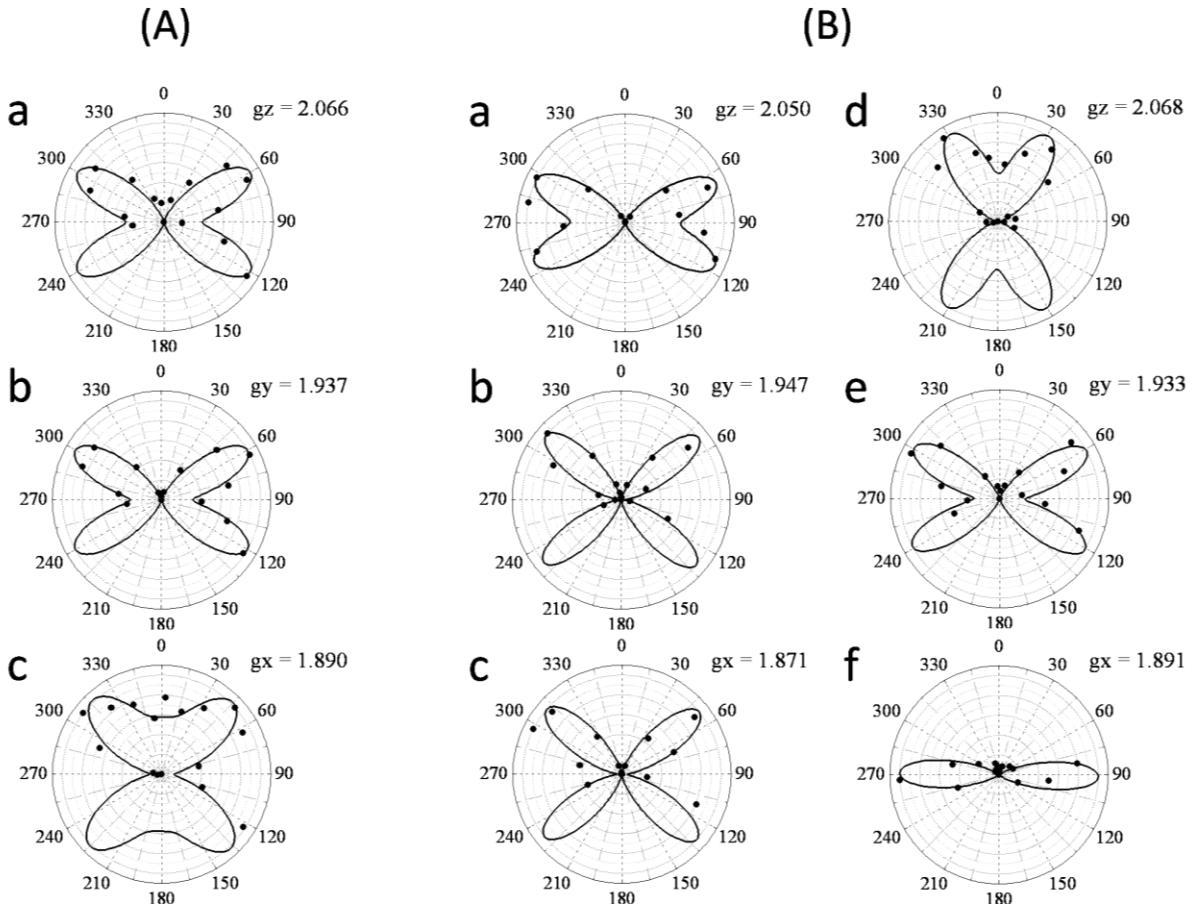

Figure 3: (A): Polar plots of signal amplitudes at magnetic fields corresponding to the g_z, g_y, and g_x values indicated in Fig.2B (*a*-*c*). θ (^{o}) is defined as in Fig. 1B. (B): Polar plots of signal amplitudes at magnetic fields for g_z, g_y, and g_x peaks of F_A^- (a-c) and g_z, g_y, and g_x peaks of F_B^- (d-f) as indicated in Fig. 2C.

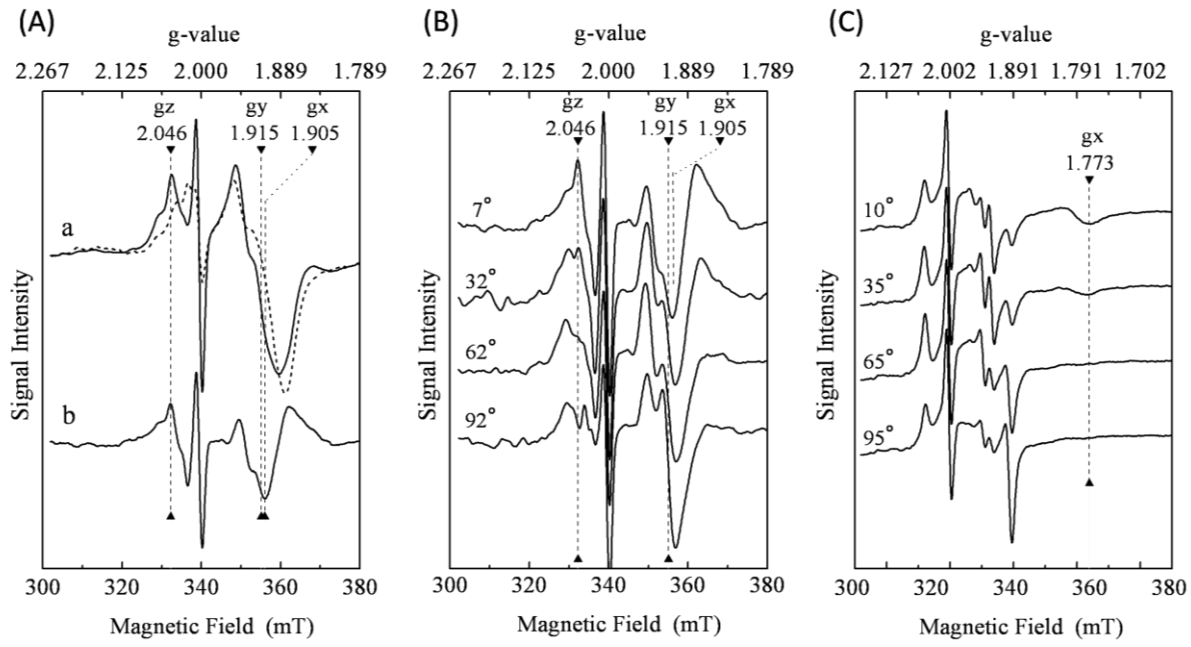

Figure 4: (A): EPR spectra of the oriented membranes of *Hbt. modesticaldum* measured in a buffer containing an excess amount of dithionite at an angle of 7° between the membrane normal and the external magnetic field. (a) Measured during illumination at 5 K (solid line) and in the dark after the illumination (broken line). (b) Light-minus-dark difference spectrum. (B): Angular dependence of the light-minus-dark (after illumination) difference spectra. Samples and experimental conditions were the same as in (A). (C): Angular dependence of EPR spectra of the oriented membrane fragments of spinach PS I frozen in the presence of an excess amount of dithionite. Spectra were measured in the dark at 14 K after preillumination at 210 K for 1 hour followed by cooling during illumination to 5 K. A triangle indicates the peak position at g_x of F_X^-. Experimental conditions for the measurements: temperature, 5 K (A and B) and 14 K (C); microwave power, 10 mW; microwave frequency, 9.517 GHz (A and B) and 9.529 GHz (C); modulation amplitude, 20 G at 100 KHz; time constant, 20 ms.

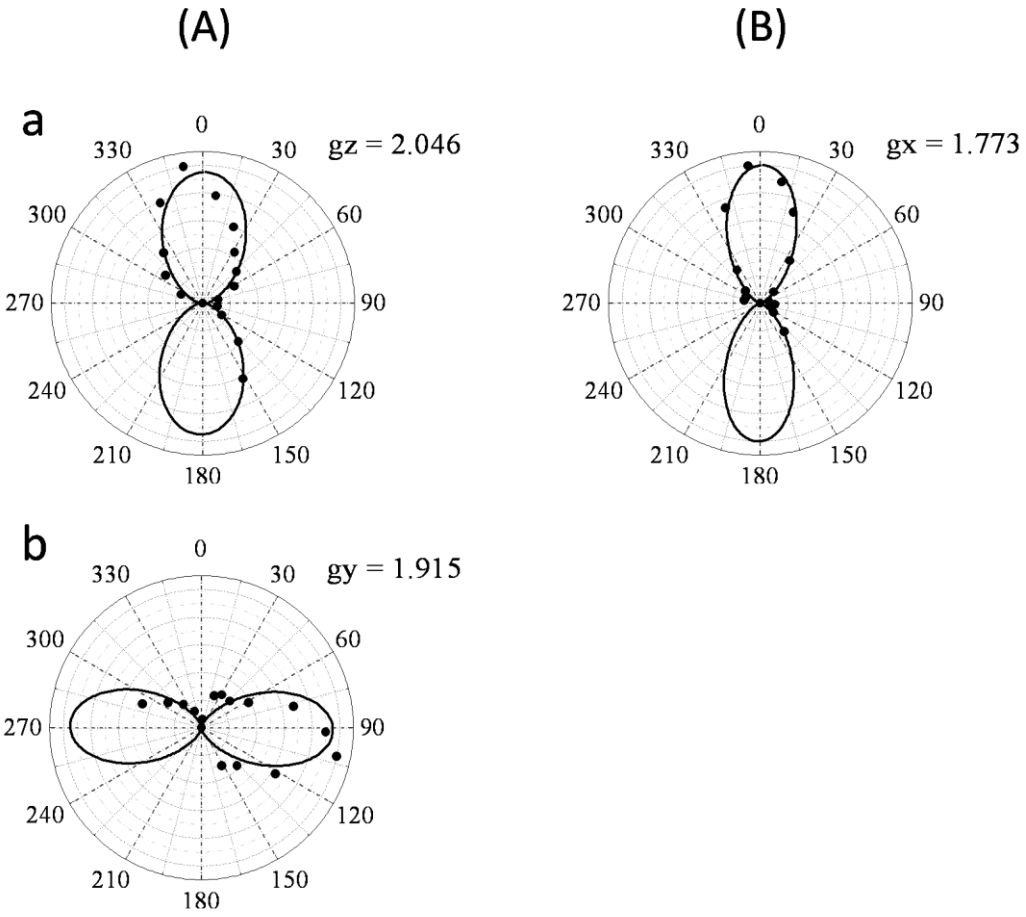

Figure 5: (A): Polar plots of signal amplitudes at magnetic fields at g_z and g_y (a, b) values as indicated by triangles in Fig.4B. θ (°) is defined as in Fig.1B. (B): Polar plots of signal amplitudes at g_x of F_X^- indicated by a triangle in Fig.4C.

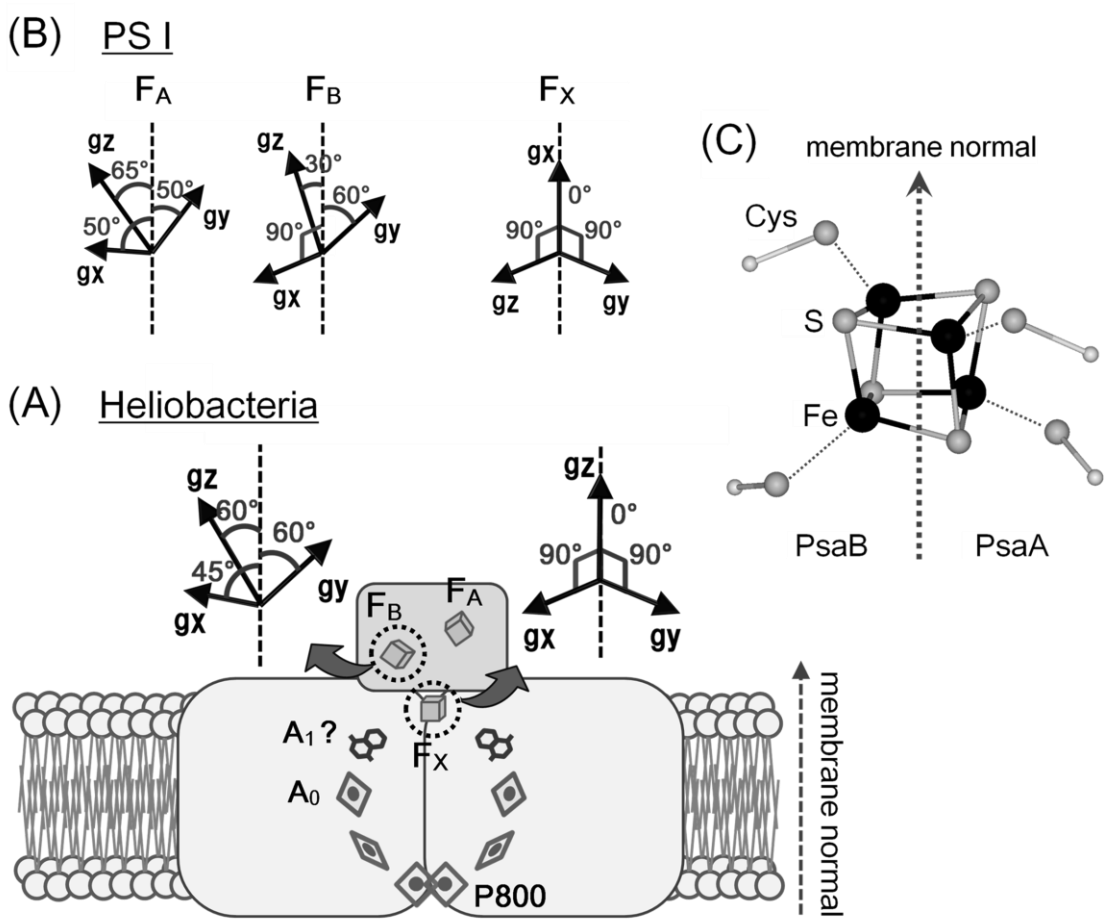

Figure 6: (A and B): Schematic models of the g-tensor orientation of FeS clusters in (A) hRC and (B) gRC, in which the hRC structure was predicted based on the homology with the PS I RC structure. The location of F_B was assumed to correspond to that of F_A in PS I because of the similarities in their orientations and redox properties (see text for details). The broken line represents the membrane normal. θ (^{o}) refers to the angle between the membrane normal and each principal axis. (C): Structure of the [4Fe-4S] cluster F_X at the center of the PsaA-PsaB heterodimeric RC of PS I, which was depicted based on the x-ray crystal structure of PS I (PDB entry 1JB0). The sulfur and C_β atoms of the two cysteins on the right belong to the PsaA polypeptide, and those of the two on the left, to PsaB. Large black, large gray, and small white spheres represent iron, sulfur, and C_β atoms, respectively. The arrowed broken line represents the membrane normal.

References

[1] Gest, H. and Favinger, J.L. (1983) *Heliobacterium chlorum*, an anoxygenic brownish-green photosynthetic bacterium containing a new form of bacteriochlorophyll, Arch. Microbiol. 136, 11-16.

[2] Woese, C.R., Debrunnervossbrinck, B.A., Oyaizu, H., Stackebrandt, E. and Ludwig, W. (1985) Gram-positive bacteria: Possible photosynthetic ancestry, Science 229, 762-765.

[3] Amesz, J. (2004) Anoxygenic Photosynthetic Bacteria (Bauer, C., Ed.), Vol. 2, pp. 687-697, Springer, Netherlands.

[4] Vandemeent, E.J., Kobayashi, M., Erkelens, C., Vanveelen, P.A., Amesz, J. and Watanabe, T. (1991) Identification of 8^1-Hydroxychlorophyll *a* as a functional reaction center pigment in heliobacteria, Biochim. Biophys. Acta 1058, 356-362.

[5] Buttner, M., Xie, D.L., Nelson, H., Pinther, W., Hauska, G. and Nelson, N. (1992) Photosynthetic reaction center genes in green sulfur bacteria and in photosystem 1 are related, Proc. Natl. Acad. Sci. USA 89, 8135-8139.

[6] Vermaas, W.F.J. (1994) Evolution of heliobacteria: Implications for photosynthetic reaction center complexes, Photosynth. Res. 41, 285-294.

[7] Olson, J.M. and Blankenship, R.E. (2004) Thinking about the evolution of photosynthesis, Photosynth. Res. 80, 373-386.

[8] Oh-oka, H. (2007) Type 1 reaction center of photosynthetic heliobacteria, Photochem. Photobiol. 83, 177-186.

[9] Heinnickel, M. and Golbeck, J.H. (2007) Heliobacterial photosynthesis, Photosynth. Res. 92, 35-53.

[10] Trost, J.T. and Blankenship, R.E. (1989) Isolation of a photoactive photosynthetic reaction center core antenna complex from *Heliobacillus mobilis*, Biochemistry 28, 9898-9904.

[11] Vandemeent, E.J., Kleinherenbrink, F.A.M. and Amesz, J. (1990) Purification and properties of an antenna reaction center complex from Heliobacteria, Biochim. Biophys. Acta 1015, 223-230.

[12] Liebl, U., Mockensturmwilson, M., Trost, J.T., Brune, D.C., Blankenship, R.E. and Vermaas, W. (1993) Single core polypeptide in the reaction center of the photosynthetic bacterium *Heliobacillus mobilis*: Structural implications and relations to other photosystems, Proc. Natl. Acad. Sci. USA 90, 7124-7128.

[13] Amunts, A., Drory, O. and Nelson, N. (2007) The structure of a plant photosystem I supercomplex at 3.4 Å resolution, Nature 447, 58-63.

[14] Jordan, P., Fromme, P., Witt, H.T., Klukas, O., Saenger, W. and Krauss, N. (2001)

Three-dimensional structure of cyanobacterial photosystem I at 2.5 Å resolution, Nature 411, 909-917.

[15] Kobayashi, M., Vandemeent, E.J., Erkelens, C., Amesz, J., Ikegami, I. and Watanabe, T. (1991) Bacteriochlorophyll *g* epimer as a possible reaction center component of heliobacteria, Biochim. Biophys. Acta 1057, 89-96.

[16] Rigby, S.E.J., Evans, M.C.W. and Heathcote, P. (2001) Electron nuclear double resonance (ENDOR) spectroscopy of radicals in photosystem I and related Type 1 photosynthetic reaction centres, Biochim. Biophys. Acta 1507, 247-259.

[17] Mizoguchi, T., Oh-oka, H. and Tamiaki, H. (2005) Determination of stereochemistry of bacteriochlorophyll g_F and 8^1-hydroxy-chlorophyll a_F from *Heliobacterium modesticaldum*, Photochem. Photobiol. 81, 666-673.

[18] Kleinherenbrink, F.A.M., Ikegami, I., Hiraishi, A., Otte, S.C.M. and Amesz, J. (1993) Electron transfer in menaquinone depleted membranes of *Heliobacterium chlorum*, Biochim. Biophys. Acta 1142, 69-73.

[19] Lin, S., Chiou, H.C. and Blankenship, R.E. (1995) Secondary electron transfer processes in membranes of *Heliobacillus mobilis*, Biochemistry 34, 12761-12767.

[20] van der Est, A., Hager-Braun, C., Leibl, W., Hauska, G. and Stehlik, D. (1998) Transient electron paramagnetic resonance spectroscopy on green-sulfur bacteria and heliobacteria at two microwave frequencies, Biochim. Biophys. Acta 1409, 87-98.

[21] Brettel, K., Leibl, W. and Liebl, U. (1998) Electron transfer in the heliobacterial reaction center: evidence against a quinone-type electron acceptor functioning analogous to A_1 in photosystem I, Biochim. Biophys. Acta 1363, 175-181.

[22] Miyamoto, R., Nlino, H., Kondo, T., Itoh, S. and Oh-Oka, H. (2008) An electron spin-polarized signal of the $P800^+A_1(Q)^-$ state in the homodimeric reaction center core complex of *Heliobacterium modesticaldum*, Biochemistry 47, 4386-4393.

[23] Heinnickel, M., Shen, G.Z. and Golbeck, J.H. (2007) Identification and characterization of PshB, the dicluster ferredoxin that harbors the terminal electron acceptors F_A and F_B in *Heliobacterium modesticaldum*, Biochemistry 46, 2530-2536.

[24] Nitschke, W., Setif, P., Liebl, U., Feiler, U. and Rutherford, A.W. (1990) Reaction center photochemistry of *Heliobacterium chlorum*, Biochemistry 29, 11079-11088.

[25] Heathcote, P., Williamssmith, D.L., Sihra, C.K. and Evans, M.C.W. (1978) The role of membrane-bound iron-sulfur centers A and B in photosystem I reaction center of spinach chloroplasts, Biochim. Biophys. Acta 503, 333-342.

[26] Prince, R.C., Gest, H. and Blankenship, R.E. (1985) Thermodynamic properties of the photochemical reaction center of *Heliobacterium chlorum*, Biochim. Biophys. Acta 810,

377-384.

[27] Smit, H.W.J., Amesz, J. and Vanderhoeven, M.F.R. (1987) Electron-transport and triplet formation in membranes of the photosynthetic bacterium *Heliobacterium chlorum*, Biochim. Biophys. Acta 893, 232-240.

[28] Kleinherenbrink, F.A.M., Chiou, H.C., Lobrutto, R. and Blankenship, R.E. (1994) Spectroscopic evidence for the presence of an iron-sulfur center similar to F_X of Photosystem I in *Heliobacillus mobilis*, Photosynth. Res. 41, 115-123.

[29] Fromme, P., Jordan, P. and Krauss, N. (2001) Structure of photosystem I, Biochim. Biophys. Acta 1507, 5-31.

[30] Prince, R.C., Crowder, M.S. and Bearden, A.J. (1980) The orientation of the magnetic axes of the membrane-bound iron-sulfur clusters of spinach chloroplasts, Biochim. Biophys. Acta 592, 323-337.

[31] Hootkins, R. and Bearden, A. (1983) The orientation of the magnetic axes of membrane-bound iron-sulfur clusters and a cytochrome *b-559* in the green halophilic alga *Dunaliella parva*, Biochim. Biophys. Acta 723, 16-29.

[32] Guigliarelli, B., Guillaussier, J., More, C., Setif, P., Bottin, H. and Bertrand, P. (1993) Structural organization of the iron-sulfur centers in *Synechocystis* 6803 Photosystem I: EPR study of oriented thylakoid membranes and analysis of the magnetic-interactions, J. Biol. Chem. 268, 900-908.

[33] Kamlowski, A., vanderEst, A., Fromme, P. and Stehlik, D. (1997) Low temperature EPR on photosystem I single crystals: Orientation of the iron-sulfur centers F_A and F_B, Biochim. Biophys. Acta 1319, 185-198.

[34] Dismukes, G.C. and Sauer, K. (1978) Orientation of membrane-bound radicals: EPR investigation of magnetically ordered spinach-chloroplasts, Biochim. Biophys. Acta 504, 431-445.

[35] Nitschke, W., Feiler, U. and Rutherford, A.W. (1990) Photosynthetic reaction center of green sulfur bacteria studied by EPR, Biochemistry 29, 3834-3842.

[36] Madigan, M.T. (1992) The family Heliobacteriaceae. In The prokaryotes, 2nd edn. (Balows, A., Trüper, H. G., Dworkin, M., Harder, W., and Schleifer, K.H., Eds), pp. 1981-1992. Springer, Berlin.

[37] Miyamoto, R., Iwaki, M., Mino, H., Harada, J., Itoh, S. and Oh-oka, H. (2006) ESR signal of the iron-sulfur center F_X and its function in the homodimeric reaction center of *Heliobacterium modesticaldum*, Biochemistry 45, 6306-6316.

[38] Oh-oka, H., Kamei, S., Matsubara, H., Iwaki, M. and Itoh, S. (1995) Two molecules of cytochrome *c* function as the electron-donors to P840 in the reaction-center complex isolated

from a green sulfur bacterium, *Chlorobium tepidum*, FEBS Lett. 365, 30-34.

[39] Ikegami, I. and Katoh, S. (1975) Enrichment of photosystem I reaction center chlorophyll from spinach-chloroplasts, Biochim. Biophys. Acta 376, 588-592.

[40] Mino, H., Satoh, J., Kawamori, A., Toriyama, K. and Zimmermann, J.L. (1993) Matrix ENDOR of tyrosine D^+ in oriented photosystem II membranes, Biochim. Biophys. Acta 1144, 426-433.

[41] Liebl, U., Rutherford, A.W. and Nitschke, W. (1990) Evidence for a unique Rieske iron-sulfur center in *Heliobacterium chlorum*, FEBS Lett. 261, 427-430.

[42] Golbeck, J.H. and Bryant, D.A. (1991) Photosystem I, vol. 16, Academic Press, San Diego.

[43] Heinnickel, M., Shen, G.Z., Agalarov, R. and Golbeck, J.H. (2005) Resolution and reconstitution of a bound Fe-S protein from the photosynthetic reaction center of *Heliobacterium modesticaldum*, Biochemistry 44, 9950-9960.

[44] Evans, M.C.W., Sihra, C.K. and Cammack, R. (1976) Properties of primary electron-acceptor in photosystem I reaction center of spinach-chloroplasts and its interaction with P700 and bound ferredoxin in various oxidation-reduction states, Biochem. J. 158, 71-77.

[45] Warden, J.T. and Golbeck, J.H. (1986) Photosystem I charge separation in the absence of center A and B. II. ESR spectral characterization of center 'X' and correlation with optical signal 'A_2', Biochim. Biophys. Acta 849, 25-31.

[46] Vassiliev, I.R., Ronan, M.T., Hauska, G. and Golbeck, J.H. (2000) The bound electron acceptors in green sulfur bacteria: Resolution of the g-tensor for the F_X iron-sulfur cluster in *Chlorobium tepidum*, Biophys. J. 78, 3160-3169.

[47] Hauska, G., Schoedl, T., Remigy, H. and Tsiotis, G. (2001) The reaction center of green sulfur bacteria, Biochim. Biophys. Acta 1507, 260-277.

[48] Setif, P. (2001) Ferredoxin and flavodoxin reduction by photosystem I, Biochim. Biophys. Acta 1507, 161-179.

[49] Brok, M., Vasmel, H., Horikx, J.T.G. and Hoff, A.J. (1986) Electron-transport components of *Heliobacterium chlorum* investigated by EPR spectroscopy at 9 and 35 GHz, FEBS Lett. 194, 322-326.

[50] Muhiuddin, I.P., Rigby, S.E.J., Evans, M.C.W., Amesz, J. and Heathcote, P. (1999) ENDOR and special TRIPLE resonance spectroscopy of photoaccumulated semiquinone electron acceptors in the reaction centers of green sulfur bacteria and heliobacteria, Biochemistry 38, 7159-7167.

[51] Schlodder, E., Falkenberg, K., Gergeleit, M. and Brettel, K. (1998) Temperature dependence of forward and reverse electron transfer from A_1^-, the reduced secondary electron acceptor in photosystem I, Biochemistry 37, 9466-9476.

[52] Shuvalov, V.A., Dolan, E. and Ke, B. (1979) Spectral and kinetic evidence for two early electron acceptors in photosystem I, Proc. Natl. Acad. Sci. USA 76, 770-773.

Function of Quinone in Type I Homodimer Reaction Center of Heliobacteria: Identification of Electron Spin-Polarized Signal of the $P800^{+}A_1^{-}$(menaquinone^{-}) radical pair

Introduction

Heliobacteria are a group of anoxygenic photosynthetic bacteria discovered in 1983 [1] and are classified as the only low-guanine/cytosine (GC) gram-positive photosynthetic bacteria [2]. They are related to cyanobacteria more closely than the other photosynthetic bacteria based on the sequences of their 16S rRNA genes [3] and photosynthetic genes [4], and have the simplest photosynthetic system made of only a Type I reaction center (RC) complex with no antenna pigment-protein complexes. Type I RCs include RCs of heliobacteria and green sulfur bacteria (designated as hRC and gRC, respectively, hereafter), and the photosystem I (PS I) RCs of higher plants, algae, and cyanobacteria. In the Type I RCs, iron sulfur clusters function as the common terminal electron acceptors, in contrast to mobile quinones employed in Type II RCs, which include purple bacterial RC (pRC) and photosystem II (PS II) RCs of higher plants, algae, and cyanobacteria. All the RCs are made of two core polypeptides that are highly homologous (heterodimer) or identical (homodimer). Electron transfer cofactors on the two core polypeptides are arranged along almost symmetrical two branches. All the RCs seem to be evolved from an ancestral homodimeric RC [5,6] based on the homologies of amino acid sequences of the RC polypeptides and on the three-dimensional structures of heterodimeric pRCs [7,8], PS II RCs [9,10] and PS I RCs [11,12].

In the Type II RCs, electron transfer occurs through the cofactors along the one branch of cofactor arrangements after the primary charge separation, while in PS I RC, which is made of two partially homologous PsaA and PsaB core polypeptides, electron transfer occurs on two symmetrical branches with different probabilities that vary depending on the organisms. On the other hand, electron transfer seems to occur evenly along cofactors symmetrically arranged as two branches in the homodimeric hRCs [13-15] and gRCs [16], which are made of identical two PshA or PscA proteins, respectively. ENDOR and FTIR studies revealed the uniform/symmetrical spin density distribution over the two BChl molecules of the oxidized special pair $P800^{+}$ as expected [17,18]. However, the structures of homodimeric RCs have not been resolved yet. The electron transfer pathways in the Type I bacterial RCs, therefore, are still unclear, especially for the roles of quinones and iron sulfur cluster F_X [19,20].

Heliobacteria has no antenna complexes and its photosynthetic system is made of only hRC complex that contains 35-40 BChl *g* molecules that give the Q_y absorption peak at 800 nm [21]. Light energy absorbed by the antenna pigments on the hRC is transferred to the special pair P800, which is a dimer of BChl *g* (probably a heterodimer of BChl *g* and its stereoisomer BChl *g'*) [17,22], and its photochemical reaction gives an electron to the primary electron acceptor A_0, which is 8^1-hydroxy-Chl *a* (8^1-OH-Chl *a*), a derivative of chlorophyll *a* [21,23]. The sequential electron transfer along the two branches meets on the terminal electron acceptor F_X, and then, reduces F_A/F_B which are [4Fe-4S] clusters ligated by cystein residues of a PshB protein [24]. The hRC structure appears to resemble that of Type I homodimeric gRC, although the gRC attaches large amounts of extra-membrane antenna pigments in the chromosomes and FMO proteins that are bound to the cytoplasmic surface of gRC [25]. In the homodimer RCs, function of contained menaquinone has not been identified yet, although phylloquinone is known to function as the secondary electron acceptor A_1 that mediates the electron transfer between A_0 and F_x in PS I RC [19,20]. In addition, the spin property of F_X in hRC has been a matter of controversy [26,27].

Amino acid sequence analysis suggested the arrangement of electron transfer cofactors on hRC to be similar to that of their counterparts in PS I RC [28]. F_X is expected to be located at the center as the anchor between the two PshA subunits, ligated by four cysteine residues of two PshA subunits as in PS I [15]. The situation is similar in the PscA/PscA homodimeric gRC [25]. Amino acid sequences of the F_X-binding site are conserved (~50 %) between hRC and PS I RC [27]. Recent laser spectroscopy experiments revealed the reduction of $P800^+$ with a time constant (t_c) of 14 ms at room temperature in the isolated hRC core complex (hRC_{cc}), that is deprived of a PshB subunit (*i.e.,* has no F_A/F_B clusters) [13]. The absorption change at 430 nm suggested the charge recombination between $P800^+$ and F_X^- with a t_c of 20 ms at cryogenic temperature [29]. We recently, assigned an EPR signal with an S=1/2 spin ground state to F_X^- in the isolated membranes of *Heliobacterium (Hbt.) modesticaldum* after the pre-reduction of F_A/F_B [27]. On the other hand, another EPR signal with an S = 3/2 spin ground state has been attributed to F_X^- in similar membrane preparations [26]. The controversy about F_X signal, therefore, still remains to be resolved.

The reported oxidation rate of A_0^- with t_c of 500-600 ps at room temperature in hRC [30,31] and gRC [32] are considerably slower than that of 20-50 ps by phylloquinone-A_1 in PS I [33,34]. No transient absorption change of A_1^- (semiquinone) was detected in the 400-470 nm region [31] despite the presence of 1.4 molecules of menaquinone per P800 in hRC [13]. Only one type of electron spin polarized (ESP) transient signal, which originates from $P800^+F_X^-$ state, has been reported at 100 K in hRC [35] in contrast to the detection of two different ESP signals of $P700^+A_1^-$ and $P700^+F_X^-$ in PS I. Photovoltage measurements indicated only two distinct steps in the electron transfer after the laser flash excitation of hRC, in contrast to the three steps ($P700 \rightarrow A_0 \rightarrow A_1 \rightarrow F_X$) in PS I [36].

Extraction of menaquinone from hRC by diethyl ether treatment induced no changes in the re-oxidation rate of A_0^- [37]. Therefore, a little evidence for the action of A_1 is emerging in hRC. However, the distance between A_0 and F_X, that is expected to be nearly 20 Å based on the crystal structure of PS I, appears to be too long to enable the "single-step" electron transfer without the action of menaquinone between them [38].

Some evidences have suggested the action of menaquinone in hRC. EPR and ENDOR studies detected the accumulation of semiquinone radical in hRC after the illumination in the presence of dithionite [39,40]. The two-phase kinetics of the transient absorption changes of P800 at 10 K might be attributed to the charge recombination from A_1^- and F_X^-, respectively [41]. The redox titration of hRC_{cc} without F_A/F_B clusters suggested that two different electron transfer cofactors (presumably menaquinone and F_X) in addition to A_0 serve as electron acceptors [38]. Recently, we detected a light-induced transient ESP signal in the purified hRC_{cc} of *Hbt. modesticaldum* that was pre-illuminated in the presence of dithionite [42]. The ESP signal exhibited an A/E/A/E (A, absorption; E, emission) pattern, and was attributed to the $P800^+A_1^-$ state. This pattern is clearly different from the E/A pattern of $P800^+F_X^-$ radical pair state [35].

In this study, we worked on the spectral and kinetically assignments of the A/E/A/E-type ESP signal of $P800^+A_1^-$ carefully. We measured this signal more correctly in pre-illuminated hRC_{cc} of *Hbt. modesticaldum* and identified it to be actually an A/E type signal. We estimated the molecular orientation of A_1 menaquinone based on the measurements using the improved pre-illumination procedure. The temperature dependences of the charge recombination of A_1^- and F_X^- with $P800^+$ were also observed in hRC_{cc}. We discuss the function of menaquinone as an electron acceptor A_1 and the electron transfer pathway including F_X and A_1 in hRC.

Materials and methods

Preparation of the RC core complex (hRC_{cc}) from Hbt. modesticaldum

Hbt. modesticaldum strain was generously provided by M. T. Madigan (Southern Illinois University, Carbondale, IL). Cells were grown anaerobically in a PYE medium in a 1 L bottle under continuous illumination with tungsten lamps [43]. To avoid the accumulation of lysed cells that increase in the late-logarithmic growth phase, cultivation was performed at 47 °C only for 18-20 h using 1% inocula [27]. All the procedures for the preparation of membranes as well as the EPR measurements were carried out under anaerobic conditions, as previously described [44]. All the media were fully degassed and flushed with N_2 gas three times and kept in an anaerobic chamber (Coy Laboratory Products, Grass Lake, MI) overnight before being used.

The membrane and hRC_{cc} preparations were isolated basically as previously described [18,27]. The cells were harvested by centrifugation at 12,000 g for 10 min, suspended in 7-8 mL of a buffer [50 mM Tris-HCl (pH 8.0), 1 mM EDTA, and 2 mM DTT], and disrupted by being passed through a French pressure cell three times at 20,000 psi. After removal of the cell debris by centrifugation at 12,000 g for 10 min, the membranes were collected by ultracentrifugation at 180,000 g for 1 h.

The hRC_{cc} was obtained after solubilization of membranes with sucrose monolaurate, and purified by stepwise sucrose density gradient centrifugation and subsequent hydrophobic chromatography. The purified hRC_{cc} gave a single PshA band with no PshB band on SDS-PAGE analysis [27]. The obtained hRC_{cc} was suspended in a buffer containing 50 mM Tris-HCl (pH 8.0), 1 mM EDTA, 2 mM DTT, and 2 mM sucrose monolaurate. For the EPR measurements, hRC_{cc} was concentrated using a Minicon-B15 apparatus (Amicon) to give an absorbance of 350–500 at 788 nm. Appropriate amounts of solid sodium dithionite and 10% (v/v) glycerol were added to the hRC_{cc} solution to enable the reduction of the cofactors by the pre-illumination. Spinach PS I RC complex, which was prepared as reported previously [45], was added with 10 % (v/v) glycerol and appropriate amounts of solid sodium ascorbate to reduce P700.

Sample conditions

EPR measurements of hRC_{cc} were done under three conditions in the presence of sufficient amount of dithionite. Firstly, hRC_{cc} suspension was cooled down to 5 K in the dark (defined as dark-cooled hRC_{cc}). Secondly, hRC_{cc} suspension was illuminated at 210 K for 1 hour, and then cooled down to 5 K under illumination (light-cooled hRC_{cc}). Thirdly, the light-cooled hRC_{cc} suspension was warmed to 210 K and dark-adapted for 1 hour, and then cooled down to 5 K in the dark again (dark-re-cooled hRC_{cc}).

EPR measurements

EPR measurements were carried out using a Bruker ESP-300E X-band spectrometer (Bruker Biospin, Germany) equipped with a liquid-helium flow cryostat and a temperature control system (CF935, Oxford Instruments, Oxford, UK) with a field modulation frequency of 100 kHz for the transient and continuous wave (CW) EPR measurements. Continuous white light illumination was given from a 500 W tungsten lamp through heat-cut glass filters and a glass fiber light guide for the pre-illumination and the CW EPR measurements of a light spectrum. Xenon flash light with a few microsecond duration of nearly saturating intensity (Sugawara X-50) was given through a 1 m glass fiber light guide at 1 Hz for the measurements of a transient EPR signal. The signals were accumulated to increase the signal-to-noise ratio.

Results

Two types of electron spin polarized EPR signals in hRC_{cc}

We measured EPR signals in the reaction center core complex hRC_{cc} of *Hbt. modesticaldum*, which is made of only PshA subunits and lacks PshB subunit that binds F_A/F_B [27]. We can expect the light-induced electron transfer from P800 to A_0, (A_1) to F_X and, then, back to $P800^+$ in hRC_{cc} [27,42]. Figure 1 shows the transient EPR spectra induced by the flash excitations at various temperatures in hRC_{cc} (A, B) and spinach PS I (C). The derivative-type spectra were measured in a field-modulation mode at 100 kHz. Transient spectra at 0 μs (closed circles, averaged for 0-20 μs) and 500 μs (open circles, for 350-650 μs) after the flash excitation are shown.

Panel A shows the spectra measured at 5-50 K of the hRC_{cc} cooled in the dark (dark-cooled hRC_{cc}). The spectra at 0 μs (closed circles) show an emissive (E) and absorptive (A) peaks, as typical for the ESP spectrum, at every temperature measured. The ESP spectrum with the E/A pattern agrees with the reported radical pair ESP signal of $P800^+F_X^-$ [35,46-48]. The amplitude and spectral shape of the E/A-ESP signal were almost the same at 5-50 K, and the signal was detectable even at 200 K (data not shown). The spectra at 500 μs (open circles) shows the thermally equilibrated spin state attained after the relaxation from the ESP state. The spectra at g = 2.002 and a line width of 1.0 mT can be assigned to the $P800^+$ signal [42].

Panel B shows the ESP spectra at 5-50 K of hRC_{cc} that was cooled to 5 K under illumination after the pre-illumination at 210 K for 1 hour (light-cooled hRC_{cc}). The 0 μs spectrum at 5 K (closed circles) shows the ESP feature with an A/E pattern that spreads over the wider region. This ESP signal, which is distinct from the E/A-ESP signal of $P800^+F_X^-$ state in panel A, was assigned to $P800^+A_1^-$ state. The signal intensity decreased at the higher temperatures, and became undetectable above 20 K remaining a small signal of $P800^+F_X^-$ as detected in the dark-cooled hRC_{cc} (panel A). The A/E-ESP signal increased again upon the re-cooling below 20 K.

The 500 μs spectrum in panel B (open circles) indicated only small extents of $P800^+$, which was about 5 % of those in panel A. Therefore, most of $P800^+$ seems to be reduced in the charge recombination reaction with A_1^- before the depolarization of spins, resulting in negligible amount of A_1^- and $P800^+$ after each flash. It is in contrast to the situation in panel A that gave the larger extents of $P800^+$ at 500 μs, suggesting the slower charge recombination rate between $P800^+$ and F_X^-. If we again dark-incubate the light-cooled hRC_{cc} at 210 K for 1 hour and cooled it down to 5 K (dark-re-cooled hRC_{cc}), then the transient spectrum at 14 K showed the E/A-ESP spectrum of $P800^+F_X^-$ (data not shown), indicating the recovery of fast electron transfer to F_X. In this case, the amount of $P800^+$ at 500 μs was about 47 % of that of the dark-cooled hRC_{cc}.

We also measured transient ESP-EPR spectra in spinach PS I that was dark-cooled in the presence of ascorbate (panel C in Fig. 1 with normalized signal amplitudes). The ESP spectrum measured at 14 K shows the E/A/E pattern that can be ascribed to $P700^+A_1^-$ state [46]. The spectral shape changed drastically at around 200 K into an E/A-ESP pattern of $P700^+F_X^-$ as seen at 245 K [46], indicating the suppression of the electron transfer from A_1-phylloquinone to F_X at the lower temperature [49,50]. Both in hRC_{cc} and PS I, ESP signals of $P^+F_X^-$ gave E/A type ESP patterns. On the other hand, $P^+A_1^-$ states of the two RCs are significantly different (1) in the ESP pattern and decay times, and (2) in the conditions of ESP formation; the A/E-ESP of $P800^+A_1^-$ was formed only in the light-cooled hRC_{cc} only below 20 K, while the E/A/E-ESP of $P700^+A_1^-$ was formed at 4-200 K even in the dark-cooled PS I.

The A/E-ESP signal was also detected in the membranes of *Hbt. modesticaldum* after the pre-illumination for 1 hour in the presence of dithionite. On the other hand, we observed a modified A/E/A/E-type ESP in the hRC_{cc} cooled after pre-illumination in the presence of ascorbate (data not shown). This signal resembled the A/E/A/E-type ESP in our previous report in the hRC_{cc} cooled after the pre-illumination in the presence of dithionite [42]. This A/E/A/E-type ESP feature, therefore, seems to come from the mixing of the E/A-ESP of $P800^+F_X^-$ to the A/E-ESP of $P800^+A_1^-$ presumably with the insufficient pre-reduction of F_X.

ESP decay and rate of charge recombination in hRC_{cc}

Figure 2 shows the flash-induced kinetics of the E/A-ESP signal of $P800^+F_X^-$ state in the dark-cooled hRC_{cc} (trace *a* in panel A, traces *a* and *b* in panel B) and the A/E-ESP signal of $P800^+A_1^-$ state in the light-cooled hRC_{cc} (trace *b* in panel A, traces *c* and *d* in panel B). Panel A compares the kinetics of the two type ESP signals measured at their negative peaks at 340.3 (*a*) and 339.3 mT (*b*) in Fig. 1, respectively. We fitted the decay of the E/A-ESP signal (*a*) with three exponential decay functions with t_cs of 90 μs, 1.2 ms, and 5.6 ms at relative amplitudes of 51, 22, and 27 %, respectively. The slower 1.2 and 5.6 ms phases were ascribed to the charge recombination between $P800^+$ and F_X^- [27,35], and the fast 90 μs one to the decay of ESP signal. The decay time course of the A/E-ESP signal (*b*), on the other hand, could be fitted only with a single exponential decay with a t_c of 70 μs. The decay seems to represent the charge recombination between $P800^+$ and A_1^- as will be discussed in more detail. The spin relaxation rate of $P800^+A_1^-$ radical pair ESP seems to be slower than the reduction/oxidation of $P800^+/A_1^-$ because only small amounts of depolarized/thermally-equilibrated spins of $P800^+$ or A_1^- remained after this decay phase. The decay time of 70 μs is comparable to the 15-150 μs charge recombination time of $P700^+A_1^-$ at 10 K in PS I [51], and obviously different from the 55 ns decay t_c of $P800^+A_0^-$ state at 5 K in hRC [52], which is too fast to be detected by the present field modulation mode EPR. Therefore, we conclude that the A/E pattern ESP signal originates from

the $P800^+A_1^-$ radical pair state and disappears mainly by the electron transfer reaction at least at 5-20 K. We can, then, assume that menaquinone-A_1 mediates the electron transfer between A_0 and F_X as does phylloquinone-A_1 in PS I. and $P800^+A_1^-$ states (*c* and *d*) at their negative peaks at 338.9 and 339.3 mT, respectively. Traces *a* and *b* were detected at 20 and 7 K, respectively.

Figure 2B shows the temperature dependent changes in the flash-induced kinetics of the two type ESP states in the μs time range. Traces *a* and *b* indicate the kinetics of the negative peak of $P800^+F_X^-$ ESP measured at 20 and 7 K, respectively, at 338.9 mT in the dark-cooled hRC_{cc}. The kinetics at 7 K (*b*) was fitted with t_cs of 115 μs (87 %) and > 1 ms (13 %), and at 20 K (*a*), similar t_cs of 120 μs (83 %) and > 1 ms (17 %). The fast phase can be ascribed to the depolarization of spins on the $P800^+F_X^-$ state, and the slow phase to the decrease of depolarized spin on $P800^+$ in the recombination reaction with F_X [27,35]. Traces *c* and *d* indicate the kinetics of the negative peak of $P800^+A_1^-$ ESP measured at 20 and 5 K, respectively, at 339.3 mT in the light-cooled hRC_{cc}. The kinetics at 5 K (*d*) was fitted with two decay phases with t_cs of 90 μs (93 %) and >1 ms (7 %). The fast phase seems to be attributed to the charge recombination between $P800^+$ and A_1^- which competes with the depolarization of spins on the $P800^+A_1^-$ state, while the slow phase seems to represent the decay of $P800^+$ produced in hRC_{cc}, in which pre-reduction of F_X was incomplete. The signal amplitude was smaller at 20 K (*c*). The decay was fitted with the 25 μs (71 %) and >1 ms (29 %) phases. The former t_c is shorter than that at 5 K.

Figure 3A shows *Arrhenius* plots of decay rates of the fast phase in the dark-cooled (closed circles) and light-cooled hRC_{cc} (open circles). The spin depolarization rate in $P800^+F_X^-$ state (closed circles) was virtually temperature independent, while the charge recombination rate in $P800^+A_1^-$ state (open circles) became faster at the higher temperature. Linear regression of the *Arrhenius* plots (dotted line in panel A) gave an apparent activation energy value of 0.7 meV, and its extrapolation predicts the 20 μs decay time of A_1^- at room temperature. Panel B shows the temperature dependences of the amplitudes of the fast decay phase in the dark-cooled (closed circles) and light-cooled hRC_{cc} (open circles). The amplitude of the $P800^+A_1^-$ ESP (open circles) became smaller on warming and became negligible above 20 K, in contrast to the temperature independent amplitude of $P800^+F_X^-$ ESP (closed circles).

Figure 4 shows the decay kinetics of the depolarized $P800^+$ monitored at its 339.4 mT peak (Fig. 1) in the ms time range with normalized peak amplitudes. Traces *a* and *b* were detected at 50 and 14 K in the dark-cooled hRC_{cc}, respectively. The decay at 14 K (trace *b*) was fitted with two t_cs of 2.3 ms (77 %) and 8.3 ms (23 %), and that at 50 K (trace *a*) with similar t_cs of 1.8 ms (69 %) and 5.8 ms (31 %). These two phases can be ascribed to the charge recombination between $P800^+$ and F_X^- [27,35]. Trace *c* and *d* show the kinetics at 50 and 14 K in the light-cooled hRC_{cc}, respectively. The signal intensities were lower than those in the dark-cooled hRC_{core} (trace *a* and *b*) as also seen in

Fig. 1. The kinetics were fitted with a little longer two t_cs of 4.5 ms (82 %) and 21.0 ms (18 %) at 14 K (*d*) and of 2.2 ms (66 %) and 11.6 ms (34 %) at 50 K (*c*). A small contribution of the $P800^+A_1^-$ ESP signal within 1 ms was ignored in this fittings.

Figure 5A shows *Arrhenius* plots of decay rates of the fast and slow phases of $P800^+$ decay in the dark-cooled and light-cooled hRC_{cc} (closed and open symbols, respectively). The plots miss the decay rates of $P800^+$ below 14 K in the light-cooled hRC_{cc} due to the overlap of the large ESP signals. Linear regressions for the data points gave apparent activation energies of 0.3 meV for the two phases in the dark-cooled hRC_{cc}. The values are very small compared to the 15-110 meV values estimated for the electron transfer rate from A_1 to F_X in PS I determined at 220-300 K [50]. The low apparent activation energy suggests the charge recombination to occur via the activationless electron tunneling process from F_X^- to $P800^+$ in hRC. In the light-cooled hRC_{cc}, similar low but a little larger activation energies of 1.0 and 0.5 meV were estimated for the fast and slow phases, respectively. Temperature dependences of the signal amplitudes in the dark- and light-cooled hRC_{cc} (panel B) were similar each other although the t_cs and the apparent activation energies in the light-cooled hRC_{cc} were larger than those in the dark-cooled hRC_{cc}.

Effects of pre-illumination on CW-EPR signals of $P800^+$ and menaquinone-A_1^-

Figure 6A shows CW EPR spectra of hRC_{cc} in a g = 2 region. Trace *a* and *b* represent the light-induced spectra obtained at 14 and 50 K induced in the dark-cooled hRC_{cc}, respectively. The both spectra show the light-induced formation of $P800^+$ radical with around g = 2.003 and a line width of 1.0 mT as reported [53]. On the other hand, the light-cooled hRC_{cc} exhibited a different type of radical (trace *c* dotted line) already in the dark at 30 K. The radical species, which gave a spectrum centered at g = 2.0062 and a line width of 1.2 mT, is different from $P800^+$, and resembles the semiquinone radical (A_1^-) detected after the pre-illumination of heliobacterial membranes in the presence of dithionite with a slightly smaller g-value of 2.0038-2.0046 [39,40]. The results indicate the stable accumulation of semiquinone as previously reported [42]. Trace *d* and *e* show the light-minus-dark difference spectra induced by the illumination at 14 and 50 K of the light-cooled hRC_{cc}, respectively. The spectrum at 14 Kgave a similar g-value of 2.0060 and line width of 1.2 mT to A_1^- (trace *c*). The result indicates that A_1^- is reversely induced partially with the decay rate slow enough to be detected by CW-EPR. Photo-induced $P800^T$ signal was also detectable at 5 K (data not shown). Therefore, the pre-illumination at moderate temperatures seemed to have accumulated F_X^-, which was invisible under the present condition, and partially accumulated semiquinone$^-$ too.

The 50 K-spectrum (trace *e*) gave g = 2.0040 and a line width of 1.0 mT, in contrast to the A_1^- signal at 14 K (trace *d*). The noisy spectrum with the smaller amplitude, thus, can be ascribed to $P800^+$. Panel B shows the temperature dependent changes of the g-value of the light-minus-dark

difference spectra measured in the dark- and light-cooled hRC_{cc} (closed and open triangles, respectively). The g-values of spectra were almost constant at around 2.003 at 10-50 K in the dark-cooled hRC_{cc} (closed triangles), and decreased gradually from 2.006 below 20 K to 2.004 at 50 K in the light-cooled hRC_{cc} (open triangles), suggesting the smaller contribution of A_1^- signal at the higher temperatures. The temperature dependent changes of the light-induced CW EPR signals agree with those of the ESP signals detected in Fig. 1.

In the dark-re-cooled hRC_{cc}, $P800^+$ signal similar to that in the dark-cooled hRC_{cc} was induced by the illumination (data not shown). No $P800^T$ features were found, indicating the fast electron transfer from A_0^- to the following electron acceptors. The results are consistent with the detection of large transient ESP signal of $P800^+F_X^-$ state in the dark-re-cooled hRC_{cc} (data not shown). Therefore, theA_1^- signal (trace *d* in panel A) was induced only by the illumination of the light-cooled hRC_{cc} but not in the dark-re-cooled hRC_{cc}. The results indicate that semiquinone-A_1^- can be photo-accumulated only after the accumulation of F_X^-.

Discussion

Detection of the A/E pattern ESP signal of $P800^+A_1^-$ radical pair

We previously reported the ESP-EPR signal with an A/E/A/E pattern in hRC_{core} of *Hbt. modesticaldum* after pre-illumination in the presence of dithionite, and assigned it to $P800^+A_1^-$ radical pair [42]. The A/E/A/E signal pattern was significantly different from the E/A/E pattern of $P700^+A_1^-$ in PS I. The difference was explained by the different orientation of quinone-A_1 molecules between these species [42]. In this study, the $P800^+A_1^-$ ESP signal exhibited the A/E pattern that is somewhat different from the A/E/A/E pattern obtained previously [42]. The discrepancy can be caused by the difference of the sample preparation. As a matter of fact, in the presence of ascorbate, an A/E/A/E pattern ESP signal was reproducibly detected after the pre-illumination of hRC_{cc} (data not shown). We assume that F_X was reduced insufficiently in the hRC_{cc} with ascorbate, which induced a mixed spectrum of $P800^+A_1^-$ and some extent of $P800^+F_X^-$. In the present study, we almost fully pre-reduced F_X by the pre-illumination with the stronger light for longer time in the presence of dithionite to suppress the photo-production of $P800^+F_X^-$ state. Consequently, we detected the large flash-induced A/E type ESP signal as shown in Fig. 1. We conclude that a newly found A/E-ESP signal in Fig. 1 originates from $P800^+A_1^-$ radical pair state in hRC_{cc}.

The E/A pattern ESP signal of $P800^+F_X^-$ state identified in hRC_c (Fig. 1A) resembles the E/A-ESP of $P700^+F_X^-$ in PS I (Fig. 1C). On the other hand, a difference was found between the $P^+A_1^-$ ESP signals with the A/E pattern in hRC_{core} and with the E/A/E pattern in PS I. In the previous study [42], the difference of the $P^+A_1^-$ ESP pattern was interpreted by different molecular orientation of A_1 between hRC and PS I based on the homology modeling suggesting more hydrophilic A_1-binding site in hRC, and the orientation of A_1 in hRC was tentatively determined with the spectral simulation. We simulated the newly obtained $P800^+A_1^-$ ESP signal with the A/E pattern to determine the orientation of A_1 in hRC in more details.

Figure 7 compares the ESP signals of $P700^+A_1^-$ (dots, panel A) and $P800^+A_1^-$ (dots, panel B) together with their spectral simulations according to the correlated coupled radical pair (CCRP) model [54,55]. The simulated spectra (solid and dotted lines) were calculated on various orientations of quinone ring plane. Parameters for the simulation of $P700^+A_1^-$ signal were obtained from the previous reports [56,57]. For the simulation of $P800^+A_1^-$ signal, we assumed *g*-values of A_1^- and $P800^+$ to be composed of the isotropic g-factor of 2.0060 and 2.0029 taken from Fig. 6A and the anisotropic g-factors for A_1^- and $P700^+$ in PS I, respectively [56]. Direction of the dipolar coupling axis (z_d) connecting $P800^+$ and A_1^- and the dipolar and isotropic spin-spin couplings (*D* and *J*) were also assumed to be the same as those of $P700^+A_1^-$ state in PS I [57]. The parameters were listed in Table I. The solid line (panel A) shows the simulated $P700^+A_1^-$ signal based on the structure depicted

on the right side of panel A, which coincides well with the experimental signal (dots). The dotted line (panel B) shows the simulated $P800^+A_1^-$ signal with the same orientation of A_1 as that in PS I, which is entirely different from the experimental one (dots). If the ring plane of quinone is perpendicular to the z_d axis as depicted on the right side of panel B, then the simulated spectrum represents the prominent negative peak around 339.3 mT as detected experimentally (solid line, panel B). On the other hand, the higher-field region cannot be matched even with orientations of quinone varied at each 15°. The disagreement might be explained by following two possibilities. One is the anisotoropy of the hyperfine and g-tensor of two molecules. In order to check the first possibility, a high-frequency EPR spectroscopy should be required. The other is the matter of the formation process of the radical pair, deeply concerning the lineshape of the ESP spectrum [35,54]. To clarify the second possibility, the precise reaction rate for the forward electron transfer between P800 and A_1 should be measured.

Electron transfer system in hRC vs. PS I

The 500-600 ps oxidation t_c of A_0^- measured at room temperature has been attributed to the electron transfer to F_X in hRC [30,31]. The detection of $P800^+A_1^-$ and $P800^+F_X^-$ ESP signals at 5 K in the present study suggests that the electron transfer from A_0 to A_1 and to F_X is fast enough to maintain the ESP state even at cryogenic temperature. An empirical law of the intra-protein electron transfer rate proposed by Moser and Dutton on the basis of Marcus' theory [58] predicts that the electron transfer rate is faster with a shorter edge-to-edge distance and the greater density of atoms between the reactants, and depends on the free energy gap of the relevant reaction as really demonstrated in the quinone exchange experiments in PS I [59] and pRC [60]. If we assume an edge-to-edge distance between A_0 and F_X in hRC to be 16 Å in analogy to PS I, then the empirical law predicts the optimum reaction time of several microseconds, but not 500-600 ps, between them. The discrepancy seems to be solved by assuming an electron mediator A_1 as has been proposed in literatures [19,20,42,61].

Phylloquinone functions as A_1 in PS I and mediates electrons between A_0 and F_X. The electron transfer from A_0 to A_1 is very fast with t_c of 30 ps, and that from A_1 to F_X occurs with t_cs around 15-200 ns (which are still fast enough to produce ESP) [62]. The latter step from A_1 to F_X limits the overall electron transfer from A_0 to F_X, and almost stops below 200 K [62]. As a result, we can detect $P700^+A_1^-$ state below 200 K as seen in Fig. 1C. On the other hand, hRC produced the $P800^+F_X^-$ ESP signal even below 200 K (Fig. 1A). The result indicates the electron transfer from A_1 to F_X is virtually temperature-independent. The feature may be explained by the position/orientation of the menaquinone-A_1, which is assumed to be somewhat different from that of the phylloquinone-A_1 in PS I based on the spectral simulation of the $P800^+A_1^-$ ESP state in this study. The homology modeling of the menaquinone-A_1 binding site also suggested the environments around menaquinone to

be different from that around phylloquinone in PS I [27]. If the arrangement in hRC leads to the shorter edge-to-edge distance between A_1 and F_X, then the orbital overlap between the reactant molecules and the probability of electron tunneling are expected to increase. The situation would result in the faster electron transfer rate from A_1 to F_X than the corresponding step in PS I as already proposed [42], and may have made it difficult to observe the functional A_1 in the hRC so far.

Charge recombination reaction between $P800^+$ and F_X^- in hRC

In PS I, the t_c of the re-oxidation of F_X^- by $P700^+$ occurs with t_c of 250 μs and 130 ms at room temperature and cryogenic temperature, respectively [63,64]. On the other hand, the charge recombination reaction between $P800^+$ and F_X^- in hRC_{cc} occurred with t_c of 2-11 ms at 5-50 K in almost temperature-independent manner (Fig. 5) as has been known [42]. The t_c values are similar to 20 ms at room temperature [29]. The fast temperature-independent reaction over 20 Å that is anomalous as the intra-protein electron transfer reaction [58], seems to be realized by the mediation by menaquinone-A_1.

A_1^- radical was accumulated by the pre-illumination of hRC_{cc} in the presence of dithionite (Fig. 6). Under this condition, flash excitation induced the ESP signal of $P800^+A_1^-$, with a small $P800^+F_X^-$ ESP signal followed by the $P800^+$ signal after the thermal equilibration of spins on $P800^+$ and F_X^- (Fig. 1). CW illumination also induced $P800^T$ signal at 5 K (data not shown). We can assume four states in the light-cooled hRC_{cc}: (1) F_X and two A_1 are pre-reduced, then illumination will induce $P800^T$ in the charge recombination between $P800^+$ and A_0^-; (2) F_X is reduced and A_1 is partially reduced, then illumination will induce the ESP signal of $P800^+A_1^-$; (3) F_X is oxidized and A_1 is partially reduced, then illumination will induce the ESP signal of $P800^+F_X^-$ and the following $P800^+$ signal; (4) F_X and two A_1 are oxidized, same as before the pre-illumination of hRC_{cc}, then illumination will induce the ESP signal of $P800^+F_X^-$ and the following $P800^+$ signal decayed with the same t_c as in the dark-cooled hRC_{cc}. The decay t_c for the small $P800^+$ signal after the thermal equilibration of spins on $P800^+$ and F_X^- in the light-cooled hRC_{cc} was about twice as slow as that estimated in the dark-cooled hRC_{cc} (Fig. 4). The result seems to suggest the $P800^+F_X^-$ ESP signal to occur in state (3), not (4), in which A_1 is partially reduced and fully oxidized, respectively. The accumulation of A_1^- might modify the redox potentials of other near cofactors and affect the charge recombination rate between $P800^+$ and F_X^-.

Charge recombination reaction between $P800^+$ and A_1^- in hRC

The charge recombination between $P800^+$ and A_1^- was assumed to occur with a t_c comparable to the observed 25-90 μs decay time of ESP at 5-20 K in hRC_{cc} in a temperature dependent manner (Fig. 3). The rough extrapolation of the rate suggests t_c to be 20 μs at room temperature. The t_c is in a similar range to t_cs of 10-150 μs obtained for the charge recombination of $P700^+A_1^-$ in PS I devoided

of the terminal acceptors F_A, F_B, and F_X [51]. However, the reaction between $P700^+$ and A_1^- in PS I occurs in a temperature independent manner [51]. On the other hand, when F_A, F_B, and F_X were pre-reduced in PS I, the charge recombination rate of $P700^+A_1^-$ depended on the temperature with the activation energies of 22 meV below 240 K and 171 meV above 240 K [65]. The two activation energies were attributed to the reoxidation of A_1^- by $P700^+$ and by A_0^-, respectively. The increase of the free energy of $P700^+A_1^-$ state, caused by the negative charge on nearby F_X^- and F_A^-/F_B^-, was suggested to modify the charge recombination rate and its route [65]. The effect of the reduced iron-sulfur cluster seems to explain the temperature dependence of the charge recombination of $P800^+A_1^-$ observed at 5-20 K in the pre-illuminated hRC_{cc} in this study, although the activation energy of 0.7 meV is considerably lower than 22 meV in PS I. The amplitude of the ESP signal became smaller at higher temperature as the acceleration of the decay rate (Fig. 3). It is probably because of the slow time resolution of the present experimental setup. Further measurement might estimate the activation energy for the charge recombination of $P800^+A_1^-$ to be higher.

The charge recombination of $P700^+A_1^-$ in PS I exhibited two phases with t_cs of 15 and 150 μs at 10 K [51]. The study with mutated PS I revealed that the electron transfer occurs along both branches of cofactors (mainly on PsaA side) in PS I [66], and the ratio between the two branches varies depending on the organisms [67,68]. However, the decay kinetics of A_1^- in hRC_{cc} showed no heterogeneity suggesting the equal rates of electron transfer along the two symmetrical branches of cofactors in hRC.

The continuous-light induced a semiquinone signal in the light-cooled hRC_{cc} below 20 K (Fig. 6). The semiquinone signal was reduced at the higher temperature (Fig. 6). It resembles the temperature dependence of the $P800^+A_1^-$ signal intensity. However, the extent of semiquinone signal with the relaxed spin was very small after the single excitation flash (Fig. 1B). The charge recombination of $P800^+A_1^-$ state, which is faster at the higher temperature, seems to prevent the photo-accumulation of A_1^-.

Conclusion

In this study, we detected the two types of ESP signals in hRC_{cc} that lacks F_A/F_B. The one is a newly identified A/E type ESP signal of $P800^+A_1^-$, which is detectable only below 20 K in the light-cooled (F_X-pre-reduced) hRC_{cc}. The feature of the ESP signal strongly suggests that menaquinone functions as the electron acceptor A_1 in hRC and that the decay rate of the ESP signal is determined by the charge recombination rate of A_1^- with $P800^+$ rather than the slower depolarization rate of radical pair spins. We could not detect the $P800^+A_1^-$ ESP above 20 K due to the fast decay of ESP. The fast ESP decay is interpreted to represent the fast rate of charge recombination reaction between $P800^+$ and A_1^- in the hRC_{cc}, in which the charge recombination is more accelerated by the

negative shift of redox potential of A_1 due to the electrostatic interaction with the negative charge on F_X^-. The second is the E/A type ESP signal of $P800^+F_X^-$ radical pair that can be seen in the dark-cooled (F_X-pre-oxidized) hRC_{cc}, i.e., under normal reaction condition. The charge recombination between $P800^+$ and F_X^- occurs with a very low activation energy in contrast to the case in the corresponding reaction between $P700^+$ and F_X^- in PS I that becomes very slow at cryogenic temperature. The detection of the $P800^+F_X^-$ ESP and the pre-reduction of F_X in the dark- and light-cooled hRC_{cc}, respectively, suggest the redox potential of A_1 to be lower than that of F_X.

We assume the electron transfer in hRC_{cc} to proceed as follows in a downhill manner in each step:

$$P800 \xrightarrow{(1)} A_0 \xrightarrow{(2)} A_1 \xrightarrow{(3)} F_X$$

At room temperature, the reactions (2) and (3) proceed with an overall t_c of 500-600 ps, which seems to mainly reflect that of reaction (2). We assume a faster t_c of reaction (3) because we could detect the ESP signal of $P800^+A_1^-$ only in the light-cooled hRC_{cc} where the reaction (3) was prevented. The rapid reaction (3) seems to occur with a low activation energy. Therefore, we observe the ESP of only $P800^+F_X^-$ in the dark-cooled hRC_{cc}. The short distance between A_1 and F_X and the smaller energy gap (smaller difference of redox potentials of A_1 and F_X) seems to increase the reaction rate (3) both in the forward and backward directions, and seems to result in the fast reversed electron flow from F_X^- to $P800^+$ mediated by A_1 as seen in the fast charge recombination reaction even at cryogenic temperatures. To enable this fast recombination, the potential gap between A_1 and F_X should not be large. This might be realized by the redox potential of menaquinone, which is more positive than that of phylloquinone (around -0.8 V [61,62]) in PS I and is close to or a little more negative than that of F_X. Rather hydrophilic environment estimated for menaquinone in hRC [27] supports this assumption.

The homodimer hRC, which has been considered as a prototype of PS I RC, was shown to have the electron transfer system that uses menaquinone as the secondary electron acceptor. The reactions of menaquinone (and also of F_X) are almost comparable to that of phylloquinone in PS I. However, its reaction is a little different from phylloquinone in PS I probably due to the different energy gaps, localizations, and molecular environments. The most specific feature of hRC shown in this study are the fast charge recombination of F_X^- with $P800^+$ even at cryogenic temperature and the temperature dependent reaction rate between A_1^- and $P800^+$. The difference seems to come from the reaction of menaquinone. PS I was evolved to protect its strong reducing power on A_1^- and F_X^- from the oxygenic atmosphere and to adapt the higher quantum energy available from under high visible light absorbed by Chl *a*. The adaptation process seems to have developed hydrophobic pockets for phylloquinone-A_1 as well as for F_X. The process also seems to have shifted their redox potential values to be more negative to fit to the stronger reducing power provided from A_0. As the result,

redox potential, reorganization energy, and arrangement of A_1 and F_X might have been optimized in PS I to be able to function even in the oxygenic atmosphere to achieve the low probability of charge recombination even under strong sunshine.

Tables

	A_1^-			P^+		
	g_x	g_y	g_z	g_x	g_y	g_z
PS I	2.0062	2.0051	2.0022	2.0030	2.0026	2.0023
Helio	2.0077	2.0066	2.0037	2.0033	2.0029	2.0026

	$\angle z_d$, $g(A_1^-)$			$\angle z_d$, $g(P^+)$		
	x_{A1}	y_{A1}	z_{A1}	x_p	y_p	z_p
PS I	0^o	90^o	90^o	83^o	55^o	36^o
Helio	90^o	90^o	0^o	83^o	55^o	36^o

Table I: The g-values and orientations of the principal g-tensor axes of A_1^- (defined as $g(A_1^-)$) and P^+ (defined as $g(P^+)$) used in the simulations for the ESP signals of $P700^+A_1^-$ in PS I and $P800^+A_1^-$ in hRC_{core}. The orientations of A_1 and P were defined by the angles of the g-tensor axe against the dipolar axis z_d. The spin-spin coupling constants of D = -0.17 mT and J = 0.001 mT were used. The isotropic g-values of A_1^- and $P800^+$ in hRC_{cc} were estimated in Fig. 6. The direction of z_d, the anisotropic g-values, and the spin-spin coupling constants were assumed to be the same as those in PS I [56,57]. The $P700^+A_1^-$ ESP signal in PS I was simulated with the parameters reported in [56,57].

Figures

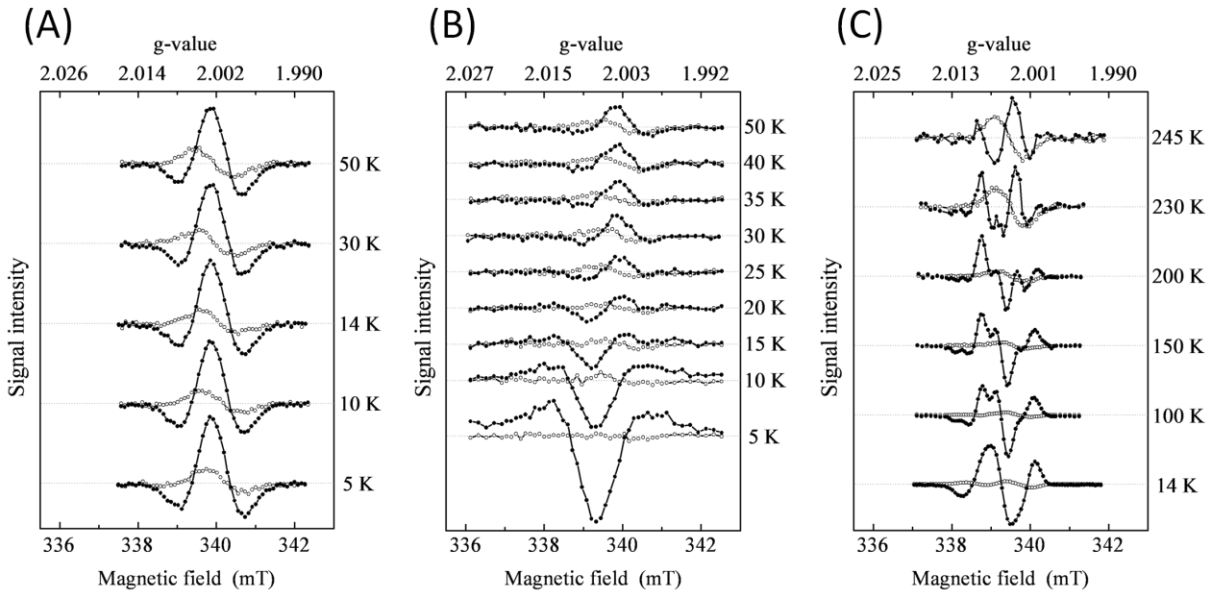

Figure 1: Temperature dependent changes of ESP-EPR spectra in hRC_{cc} of *Hbt. modesticaldum* frozen in the presence of an excess dithionite. The ESP signals were obtained in the dark-cooled (A), the light-cooled hRC_{cc} (B), and spinach PS I (C). The dark-cooled hRC_{cc} was prepared after cooling to 5 K in the dark, and the light-cooled hRC_{cc} after pre-illumination at 210 K for 1 hour and then cooling to 5 K during illumination. Closed and open circles represent the transient spectra measured at 0 μs (averaged signal intensity at 0 to 20 μs) and 500 μs (at 350 to 650 μs) after the flash excitation, respectively. The spectra in panel C were normalized. Experimental conditions: microwave power, 1 mW; microwave frequency, 9.527 (A), 9.533 (B) and 9.538 GHz (C); modulation amplitude of 0.4 mT at 100 KHz modulation; t_c, 0.01 ms.

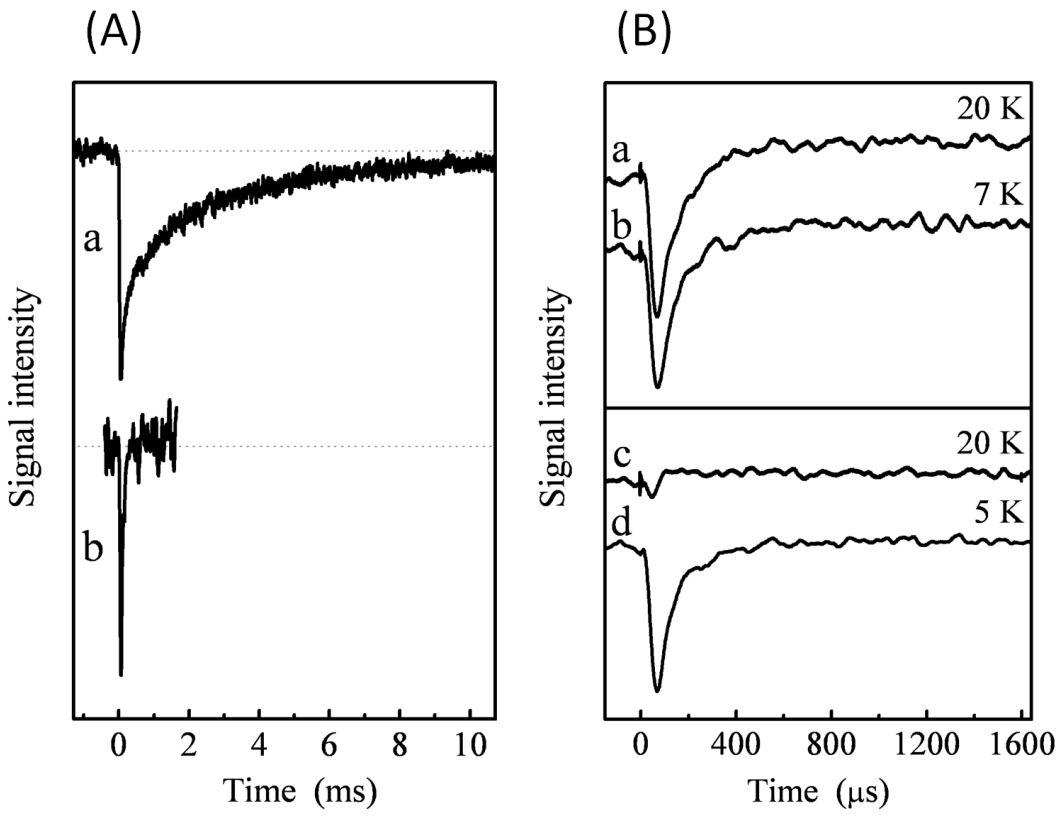

Figure 2: Flash-induced kinetics of the ESP signals in hRC_{cc}. (A): Comparison between the kinetics of the $P800^{+}F_X^{-}$ (*a*) and the $P800^{+}A_1^{-}$ signals (*b*), observed at 14 K in the dark-cooled and the light-cooled hRC_{cc}, respectively. The traces were obtained at the negative peak of the ESP signal at 340.3 and 339.3 mT, respectively. The signal amplitudes were normalized. (B): Temperature dependent changes in the kinetics of the $P800^{+}F_X^{-}$ (*a* and *b*) and the $P800^{+}A_1^{-}$ ESP signals (*c* and *d*) in the μs time range. Traces *a* and *b* were observed at 20 and 7 K, respectively, in the dark-cooled hRC_{cc} at the negative peak of $P800^{+}F_X^{-}$ ESP at 338.9 mT. Traces *c* and *d* were observed at 20 and 5 K, respectively, in the light-cooled hRC_{cc} at the negative peak of $P800^{+}A_1^{-}$ ESP at 339.3 mT. Experimental conditions: microwave power, 1 mW; microwave frequency, 9.533 GHz; modulation amplitude, 0.4 mT at 100 KHz; t_c, 0.01 ms.

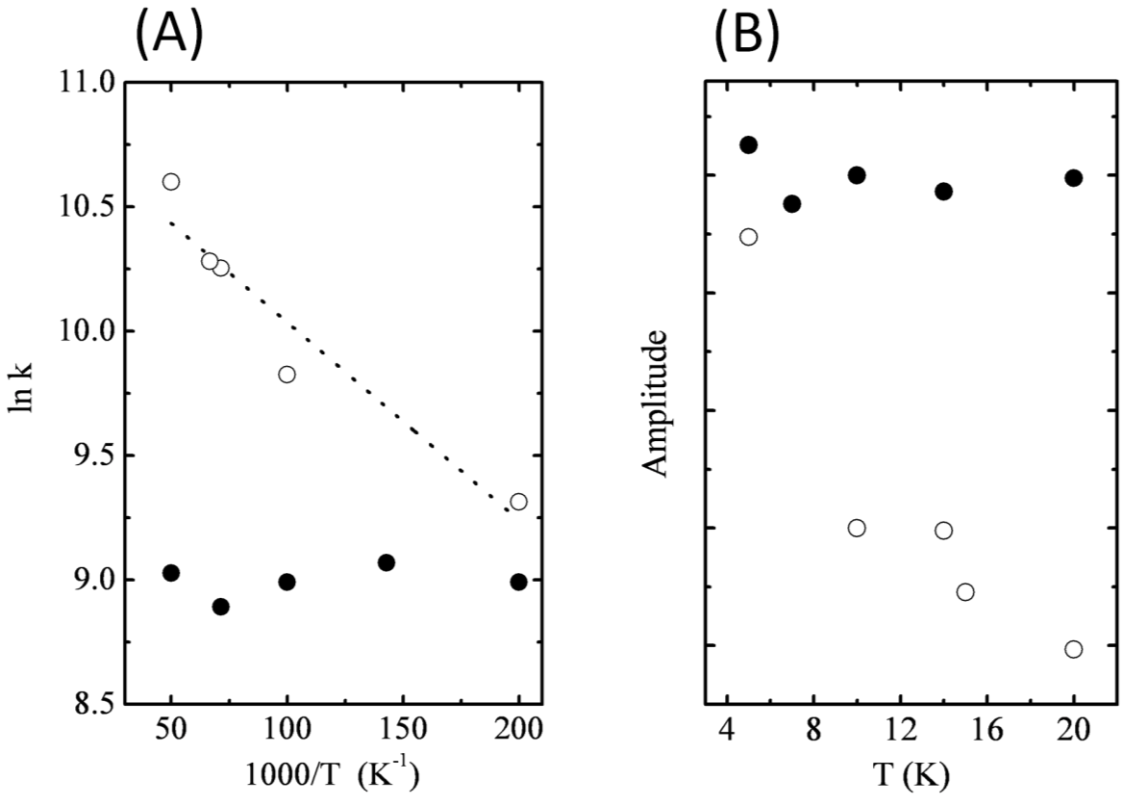

Figure 3: (A): *Arrhenius* plots of the decay rate constant *k* for the faster phase, estimated from two-exponential fits of the decay kinetics of the $P800^{+}F_X^{-}$ (closed circles) and the $P800^{+}A_1^{-}$ ESP signals (open circles), detected in the dark-cooled and the light-cooled hRC_{cc}, respectively. The dotted line represents a linear regression. (B): Temperature dependence of the amplitude of the decay phase in panel A. Experimental conditions were the same as those in Fig. 2.

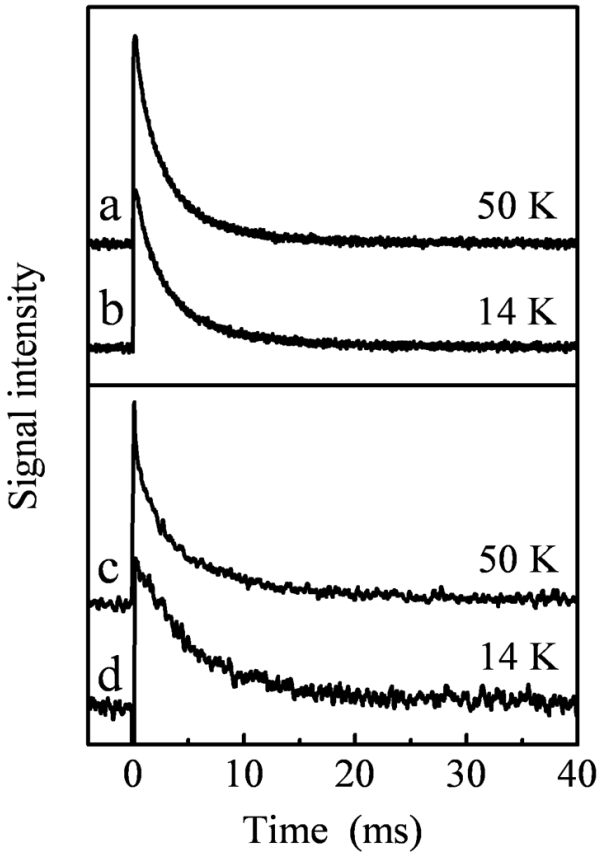

Figure 4: Temperature dependent changes in the kinetics at the positive peak of the $P800^{+}$ signal at 339.4 mT, monitored in the ms time range. Traces *a* and *b* were observed at 50 and 14 K in the dark-cooled hRC_{cc}, respectively. Traces *c* and *d* were observed at 50 and 14 K in the light-cooled hRC_{cc}, respectively. Experimental conditions: microwave power, 1 mW; microwave frequency, 9.527 GHz; modulation amplitude, 0.8 mT at 100 KHz; t_c, 0.01 ms.

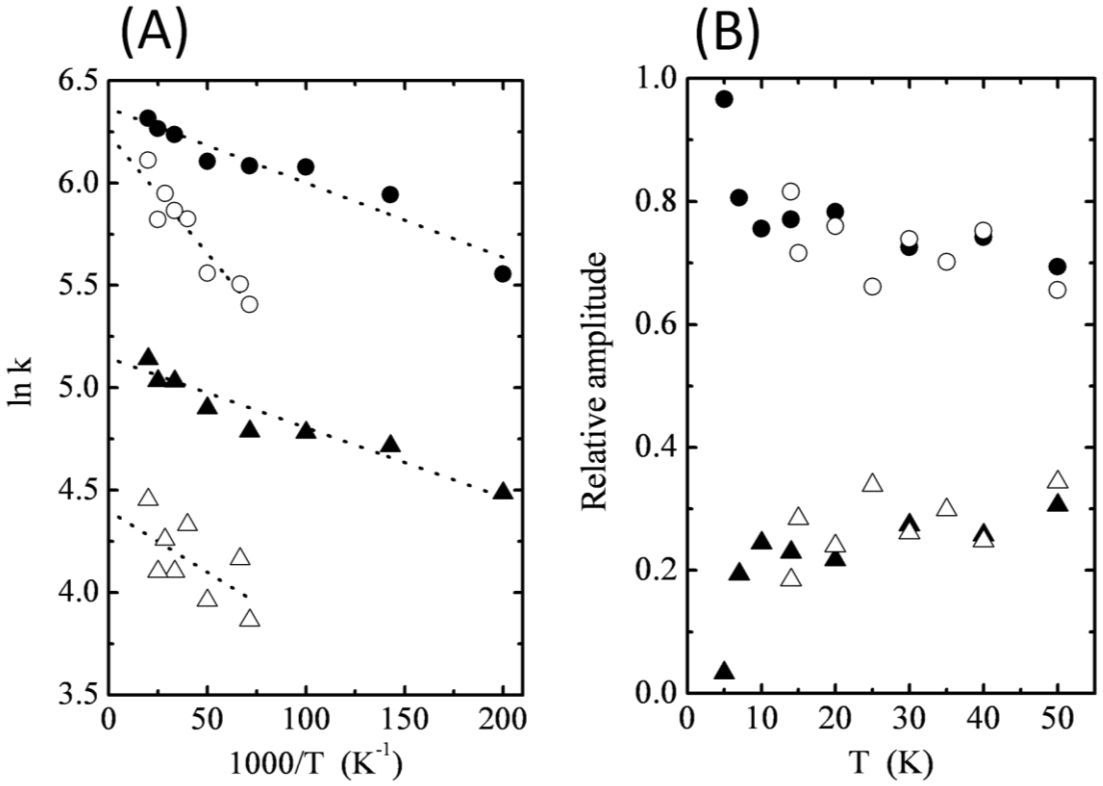

Figure 5: (A): *Arrhenius* plots of the decay rate constant *k* for the fast and slow phases, estimated from two-exponential fits of the decay kinetics of the $P800^{+}$ signal in the dark-cooled (closed symbols) and the light-cooled hRC_{cc} (open symbols). The fast and slow phases were defined as circles and triangles, respectively. The dotted lines represent linear regressions. (B): Temperature dependence of the relative amplitudes between the fast and slow phases in panel A. Experimental conditions were the same as those in Fig. 4.

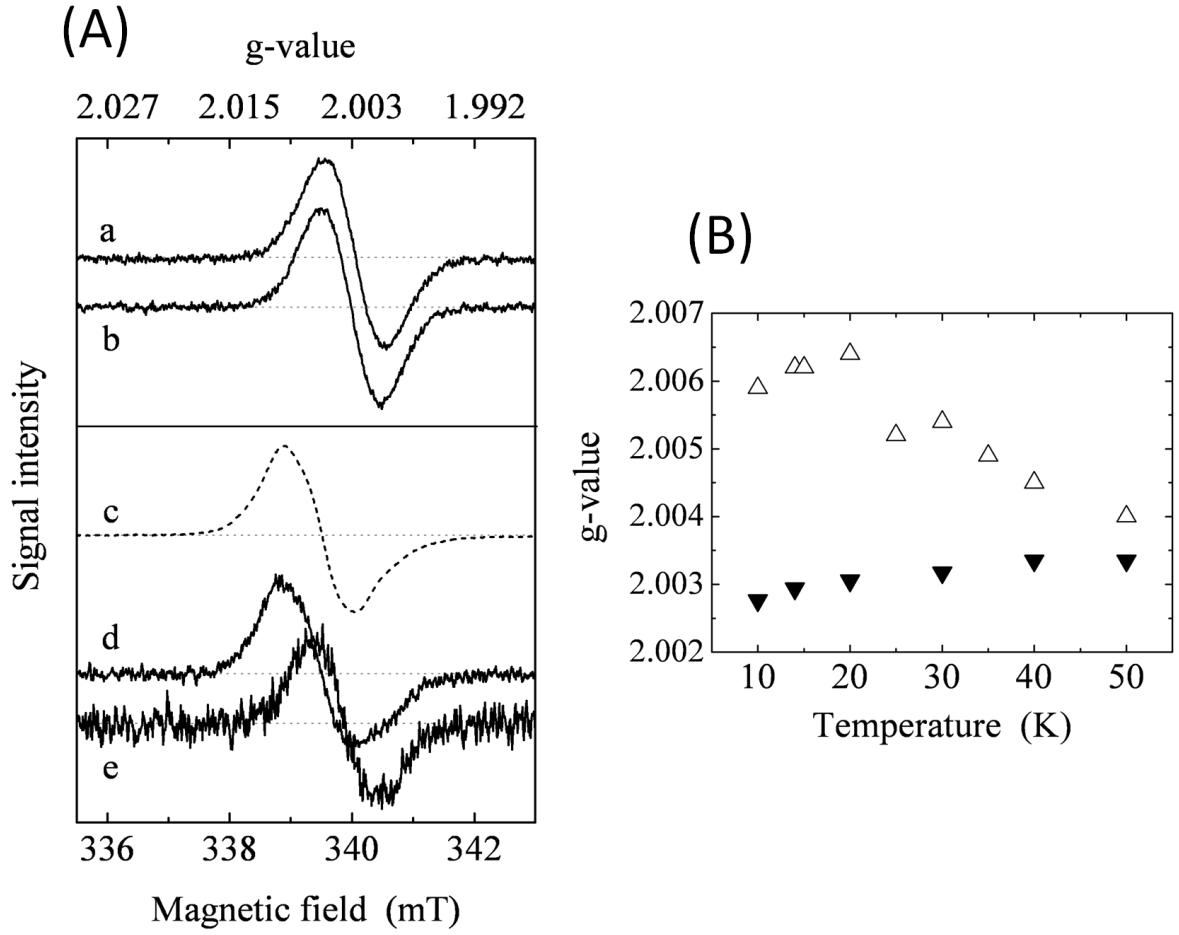

Figure 6: (A): Temperature dependent changes in CW EPR spectra in the dark-cooled (*a* and *b*) and the light-cooled hRC_{cc} (*c*-*d*). Traces *a, b, d,* and *e* represent the light-minus-dark difference spectra at 14 (*a* and *d*), 50 K (*b* and *e*), obtained by subtraction of the spectra measured in the dark after the illumination from the spectra measured during the illumination. The dotted line (trace *c*) represents the dark spectrum at 30 K after in the light-cooled hRC_{cc}. The signal intensities were normalized at their maximum peaks. (B): Temperature dependent shifts of the g-value of the light-induced spectra in the dark-cooled (closed triangles) and the light-cooled hRC_{cc} (open triangles). Experimental conditions: microwave power of 1 mW; microwave frequency of 9.533 GHz; modulation amplitude of 0.4 mT at 100 KHz; t_c, 20 ms.

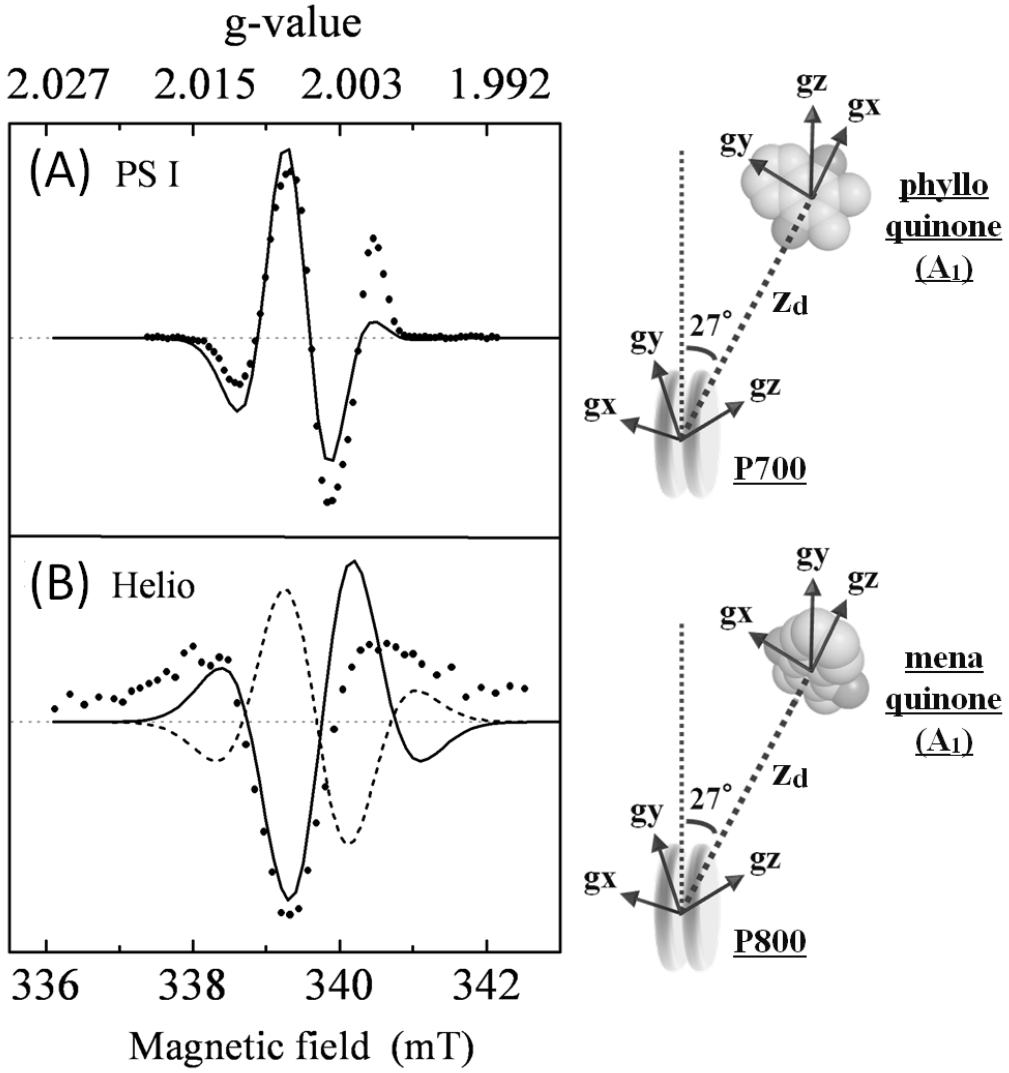

Figure 7: ESP spectra of the $P^+A_1^-$ radical pair state in PS I (A) and in hRC (B). The dots represent the experimental spectra of $P700^+A_1^-$ and $P800^+A_1^-$ states in the species. The solid lines show simulated spectra calculated based on the relative arrangement of P^+ and A_1^- in PS I and hRC as depicted on the right side of panel A and B, respectively. Note that the direction of g_z axis of the quinone molecule in the hRC is modified to be parallel to be parallel to the dipolar principal axis z_d. Parameters for the simulations were listed in Table I. The dotted line (panel B) shows the simulated $P800^+A_1^-$ ESP spectrum calculated with the same A_1-orientation as in PS I.

References

[1] Gest, H. and Favinger, J.L. (1983) *Heliobacterium chlorum*, an anoxygenic brownish green photosynthetic bacterium containing a new form of bacteriochlorophyll, Arch. Microbiol. 136, 11-16.

[2] Woese, C.R., Debrunnervossbrinck, B.A., Oyaizu, H., Stackebrandt, E. and Ludwig, W. (1985) Gram-positive bacteria: Possible photosynthetic ancestry, Science 229, 762-765.

[3] Blankenship, R.E. (1992) Origin and early evolution of photosynthesis, Photosynth. Res. 33, 91-111.

[4] Xiong, J., Fischer, W.M., Inoue, K., Nakahara, M. and Bauer, C.E. (2000) Molecular evidence for the early evolution of photosynthesis, Science 289, 1724-1730.

[5] Vermaas, W.F.J. (1994) Evolution of heliobacteria: Implications for photosynthetic reaction center complexes, Photosynth. Res. 41, 285-294.

[6] Olson, J.M. and Blankenship, R.E. (2004) Thinking about the evolution of photosynthesis, Photosynth. Res. 80, 373-386.

[7] Deisenhofer, J., Epp, O., Miki, K., Huber, R. and Michel, H. (1985) Structure of the protein subunits in the photosynthetic reaction center of *Rhodopseudomonas viridis* at 3 Å resolution, Nature 318, 618-624.

[8] Xu, Q., Axelrod, H.L., Abresch, E.C., Paddock, M.L., Okamura, M.Y. and Feher, G. (2004) X-ray structure determination of three mutants of the bacterial photosynthetic reaction centers from *Rb. sphaeroides*: Altered proton transfer pathways, Structure 12, 703-715.

[9] Loll, B., Kern, J., Saenger, W., Zouni, A. and Biesiadka, J. (2005) Towards complete cofactor arrangement in the 3.0 Å resolution structure of photosystem II, Nature 438, 1040-1044.

[10] Iwata, S. and Barber, J. (2004) Structure of photosystem II and molecular architecture of the oxygen-evolving centre, Curr. Opin. Struc. Biol. 14, 447-453.

[11] Jordan, P., Fromme, P., Witt, H.T., Klukas, O., Saenger, W. and Krauss, N. (2001) Three-dimensional structure of cyanobacterial photosystem I at 2.5 Å resolution, Nature 411, 909-917.

[12] Amunts, A., Drory, O. and Nelson, N. (2007) The structure of a plant photosystem I supercomplex at 3.4 Å resolution, Nature 447, 58-63.

[13] Trost, J.T. and Blankenship, R.E. (1989) Isolation of a photoactive photosynthetic reaction center core antenna complex from *Heliobacillus mobilis*, Biochemistry 28, 9898-9904.

[14] Vandemeent, E.J., Kleinherenbrink, F.A.M. and Amesz, J. (1990) Purification and properties of an antenna reaction center complex from heliobacteria, Biochim. Biophys. Acta 1015, 223-230.

[15] Liebl, U., Mockensturmwilson, M., Trost, J.T., Brune, D.C., Blankenship, R.E. and Vermaas, W. (1993) Single core polypeptide in the reaction center of the photosynthetic bacterium *Heliobacillus mobilis*: Structural implications and relations to other photosystems, Proc. Natl. Acad. Sci. USA 90, 7124-7128.

[16] Buttner, M., Xie, D.L., Nelson, H., Pinther, W., Hauska, G. and Nelson, N. (1992) Photosynthetic reaction center genes in green sulfur bacteria and in photosystem 1 are related, Proc. Natl. Acad. Sci. USA 89, 8135-8139.

[17] Rigby, S.E.J., Evans, M.C.W. and Heathcote, P. (2001) Electron nuclear double resonance (ENDOR) spectroscopy of radicals in photosystem I and related Type 1 photosynthetic reaction centres, Biochim. Biophys. Acta 1507, 247-259.

[18] Noguchi, T., Fukami, Y., Oh-oka, H. and Inoue, Y. (1997) Fourier transform infrared study on the primary donor P798 of Heliobacterium modesticaldum: Cysteine S-H coupled to P798 and molecular interactions of carbonyl groups, Biochemistry 36, 12329-12336.

[19] Oh-oka, H. (2007) Type 1 reaction center of photosynthetic heliobacteria, Photochem. Photobiol. 83, 177-186.

[20] Heinnickel, M. and Golbeck, J.H. (2007) Heliobacterial photosynthesis, Photosynth. Res. 92, 35-53.

[21] Vandemeent, E.J., Kobayashi, M., Erkelens, C., Vanveelen, P.A., Amesz, J. and Watanabe, T. (1991) Identification of 8^1-Hydroxychlorophyll *a* as a functional reaction center pigment in heliobacteria, Biochim. Biophys. Acta 1058, 356-362.

[22] Kobayashi, M., Vandemeent, E.J., Erkelens, C., Amesz, J., Ikegami, I. and Watanabe, T. (1991) Bacteriochlorophyll *g* epimer as a possible reaction center component of heliobacteria, Biochim. Biophys. Acta 1057, 89-96.

[23] Mizoguchi, T., Oh-Oka, H. and Tamiaki, H. (2005) Determination of stereochemistry of bacteriochlorophyll g_F and 8^1-hydroxy-chlorophyll a_F from *Heliobacterium modesticaldum*, Photochem. Photobiol. 81, 666-673.

[24] Heinnickel, M., Shen, G.Z. and Golbeck, J.H. (2007) Identification and characterization of PshB, the dicluster ferredoxin that harbors the terminal electron acceptors F_A and F_B in *Heliobacterium modesticaldum*, Biochemistry 46, 2530-2536.

[25] Hauska, G., Schoedl, T., Remigy, H. and Tsiotis, G. (2001) The reaction center of green sulfur bacteria, Biochim. Biophys. Acta 1507, 260-277.

[26] Heinnickel, M., Agalarov, R., Svensen, N., Krebs, C. and Golbeck, J.H. (2006) Identification of F_X in the heliobacterial reaction center as a [4Fe-4S] cluster with an S = 3/2 ground spin state, Biochemistry 45, 6756-6764.

[27] Miyamoto, R., Iwaki, M., Mino, H., Harada, J., Itoh, S. and Oh-oka, H. (2006) ESR signal of

the iron-sulfur center F_X and its function in the homodimeric reaction center of *Heliobacterium modesticaldum*, Biochemistry 45, 6306-6316.

[28] Fromme, P., Jordan, P. and Krauss, N. (2001) Structure of photosystem I, Biochim. Biophys. Acta 1507, 5-31.

[29] Kleinherenbrink, F.A.M., Chiou, H.C., Lobrutto, R. and Blankenship, R.E. (1994) Spectroscopic evidence for the presence of an iron-sulfur center similar to F_X of Photosystem I in *Heliobacillus mobilis*, Photosynth. Res. 41, 115-123.

[30] Nuijs, A.M., Vandorssen, R.J., Duysens, L.N.M. and Amesz, J. (1985) Excited-states and primary photochemical reactions in the photosynthetic bacterium *Heliobacterium chlorum*, Proc. Natl. Acad. Sci. USA 82, 6865-6868.

[31] Lin, S., Chiou, H.C. and Blankenship, R.E. (1995) Secondary-electron transfer processes in membranes of *Heliobacillus mobilis*, Biochemistry 34, 12761-12767.

[32] Nuijs, A.M., Vasmel, H., Joppe, H.L.P., Duysens, L.N.M. and Amesz, J. (1985) Excited-states and primary charge separation in the pigment system of the green photosynthetic bacterium *Prosthecochloris aestuarii* as studied by picosecond absorbance difference spectroscopy, Biochim. Biophys. Acta 807, 24-34.

[33] Hastings, G., Kleinherenbrink, F.A.M., Lin, S., Mchugh, T.J. and Blankenship, R.E. (1994) Observation of the reduction and reoxidation of the primary electron acceptor in photosystem I, Biochemistry 33, 3193-3200.

[34] Kumazaki, S., Iwaki, M., Ikegami, I., Kandori, H., Yoshihara, K. and Itoh, S. (1994) Rates of primary electron-transfer reactions in the photosystem I reaction center reconstituted with different quinones as the secondary acceptor, J. Phys. Chem. 98, 11220-11225.

[35] van der Est, A., Hager-Braun, C., Leibl, W., Hauska, G. and Stehlik, D. (1998) Transient electron paramagnetic resonance spectroscopy on green sulfur bacteria and heliobacteria at two microwave frequencies, Biochim. Biophys. Acta 1409, 87-98.

[36] Brettel, K., Leibl, W. and Liebl, U. (1998) Electron transfer in the heliobacterial reaction center: evidence against a quinone-type electron acceptor functioning analogous to A_1 in photosystem I, Biochim. Biophys. Acta 1363, 175-181.

[37] Kleinherenbrink, F.A.M., Ikegami, I., Hiraishi, A., Otte, S.C.M. and Amesz, J. (1993) Electron-transfer in menaquinone-depleted membranes of *Heliobacterium chlorum*, Biochim. Biophys. Acta 1142, 69-73.

[38] Trost, J.T., Brune, D.C. and Blankenship, R.E. (1992) Protein sequences and redox titrations indicate that the electron acceptors in reaction centers from heliobacteria are similar to photosystem I, Photosynth. Res. 32, 11-22.

[39] Brok, M., Vasmel, H., Horikx, J.T.G. and Hoff, A.J. (1986) Electron-transport components of

Heliobacterium chlorum investigated by EPR spectroscopy at 9 and 35 GHz, FEBS Lett. 194, 322-326.

[40] Muhiuddin, I.P., Rigby, S.E.J., Evans, M.C.W., Amesz, J. and Heathcote, P. (1999) ENDOR and special TRIPLE resonance spectroscopy of photoaccumulated semiquinone electron acceptors in the reaction centers of green sulfur bacteria and heliobacteria, Biochemistry 38, 7159-7167.

[41] Nitschke, W., Setif, P., Liebl, U., Feiler, U. and Rutherford, A.W. (1990) Reaction center photochemistry of *Heliobacterium chlorum*, Biochemistry 29, 11079-11088.

[42] Miyamoto, R., Nlino, H., Kondo, T., Itoh, S. and Oh-Oka, H. (2008) An electron spin-polarized signal of the $P800^{+}A_1(Q)^{-}$ state in the homodimeric reaction center core complex of *Heliobacterium modesticaldum*, Biochemistry 47, 4386-4393.

[43] Madigan, M.T. (1992) The family Heliobacteriaceae. In *The prokaryotes, 2nd edn.* (Balows, A., Trüper, H. G., Dworkin, M., Harder, W., and Schleifer, K.H., Eds), pp. 1981-1992. Springer, Berlin.

[44] Oh-oka, H., Kamei, S., Matsubara, H., Iwaki, M. and Itoh, S. (1995) Two molecules of cytochrome *c* function as the electron-donors to P840 in the reaction-center complex isolated from a green sulfur bacterium, *Chlorobium tepidum*, FEBS Lett. 365, 30-34.

[45] Ikegami, I. and Katoh, S. (1975) Enrichment of photosystem I reaction center chlorophyll from spinach-chloroplasts, Biochim. Biophys. Acta 376, 588-592.

[46] van der Est, A. (2001) Light-induced spin polarization in type I photosynthetic reaction centres, Biochim. Biophys. Acta 1507, 212-225.

[47] Kandrashkin, Y. and van der Est, A. (2001) A new approach to determining the geometry of weakly coupled radical pairs from their electron spin polarization patterns, Spectrochim. Acta A 57, 1697-1709.

[48] Kandrashkin, Y.E., Vollmann, W., Stehlik, D., Salikhov, K. and Van der Est, A. (2002) The magnetic field dependence of the electron spin polarization in consecutive spin correlated radical pairs in type I photosynthetic reaction centres, Mol. Phys. 100, 1431-1443.

[49] Schlodder, E., Falkenberg, K., Gergeleit, M. and Brettel, K. (1998) Temperature dependence of forward and reverse electron transfer from A_1^{-}, the reduced secondary electron acceptor in photosystem I, Biochemistry 37, 9466-9476.

[50] Agalarov, R. and Brettel, K. (2003) Temperature dependence of biphasic forward electron transfer from the phylloquinone(s) A(1) in photosystem I: only the slower phase is activated, Biochim. Biophys. Acta 1604, 7-12.

[51] Brettel, K. and Golbeck, J.H. (1995) Spectral and kinetic characterization of electron acceptor A_1 in a Photosystem I core devoid of iron-sulfur centers F_X, F_B and F_A, Photosynth. Res. 45,

183-193.

[52] Kleinherenbrink, F.A.M., Aartsma, T.J. and Amesz, J. (1991) Charge separation and formation of bacteriochlorophyll triplets in *Heliobacterium chlorum*, Biochim. Biophys. Acta 1057, 346-352.

[53] Prince, R.C., Gest, H. and Blankenship, R.E. (1985) Thermodynamic properties of the photochemical reaction center of *Heliobacterium chlorum*, Biochim. Biophys. Acta 810, 377-384.

[54] Hore, P.J. (1989) Analysis of polarized EPR spectra. in *Advanced EPR, Applications in Biology and Biochemistry* (Hoff, A.J., Ed.), pp. 405-440, Elsevier, Amsterdam.

[55] Stehlik, D., Bock, C.H. and Petersen, J. (1989) Anisotropic electron-spin polarization of correlated spin pairs in photosynthetic reaction centers, J. Phys. Chem. 93, 1612-1619.

[56] Kamlowski, A., Zech, S.G., Fromme, P., Bittl, R., Lubitz, W., Witt, H.T. and Stehlik, D. (1998) The radical pair state $P700^{+}A_1^{-}$ in photosystem I single crystals: Orientation dependence of the transient spin-polarized EPR spectra, J. Phys. Chem. B 102, 8266-8277.

[57] Zech, S.G., Hofbauer, W., Kamlowski, A., Fromme, P., Stehlik, D., Lubitz, W. and Bittl, R. (2000) A structural model for the charge separated state $P700^{+}A_1^{-}$ in photosystem I from the orientation of the magnetic interaction tensors, J. Phys. Chem. B 104, 9728-9739.

[58] Moser, C.C. and Dutton, P.L. (2006) Application of Marcus theory to photosystem I electron transfer. in *Photosystem I; The Light Driven Plastocyanin: Ferredoxin Oxidoreductase in Photosynthesis* vol. 24, pp. 583-594, Springer, Dordrecht.

[59] Iwaki, M., Kumazaki, S., Yoshihara, K., Erabi, T. and Itoh, S. (1996) Delta G_0 dependence of the electron transfer rate in the photosynthetic reaction center of plant photosystem I: Natural optimization of reaction between chlorophyll *a* (A_0) and quinone, J. Phys. Chem. 100, 10802-10809.

[60] Moser, C.C. and Dutton, P.L. (1992) Engineering protein-structure for electron-transfer function in photosynthetic reaction centers, Biochim. Biophys. Acta. 1101, 171-176.

[61] Itoh, S., Iwaki, M. and Ikegami, I. (2001) Modification of photosystem I reaction center by the extraction and exchange of chlorophylls and quinones, Biochim. Biophys. Acta. 1507, 115-138.

[62] Brettel, K. and Leibl, W. (2001) Electron transfer in photosystem I, Biochim. Biophys. Acta. 1507, 100-114.

[63] Sauer, K., Mathis, P., Acker, S. and Vanbest, J.A. (1978) Electron-acceptors associated with P700 in triton solubilized photosystem I particles from spinach-chloroplasts, Biochim. Biophys. Acta. 503, 120-134.

[64] Shuvalov, V.A., Dolan, E. and Ke, B. (1979) Spectral and kinetic evidence for two early

electron acceptors in photosystem I, Proc. Natl. Acad. Sci. USA 76, 770-773.

[65] Polm, M. and Brettel, K. (1998) Secondary pair charge recombination in photosystem I under strongly reducing conditions: Temperature dependence and suggested mechanism, Biophys. J. 74, 3173-3181.

[66] Li, Y.J. et al. (2006) Directing electron transfer within photosystem I by breaking H-bonds in the cofactor branches, Proc. Natl. Acad. Sci. USA 103, 2144-2149.

[67] Xu, W. et al. (2003) Electron transfer in cyanobacterial photosystem I. II. Determination of forward electron transfer rates of site-directed mutants in a putative electron transfer pathway from A_0 through A_1 to F_X, J. Biol. Chem. 278, 27876-27887.

[68] Ramesh, V.M., Gibasiewicz, K., Lin, S., Bingham, S.E. and Webber, A.N. (2004) Bidirectional electron transfer in photosystem I: Accumulation of A_0^- in A-side or B-side mutants of the axial ligand to chlorophyll A_0, Biochemistry 43, 1369-1375.

Publication list

1. Parallel electron donation pathways to cytochrome c_z in the type I homodimeric photosynthetic reaction center complex of *Chlorobium tepidum*
   Y. Tsukatani, C. Azai, T. Kondo, S. Itoh, H. Oh-oka, (2008), *Biochim. Biophys. Acta* 1777, 1211–1217.

2. An electron spin-polarized signal of the $P800^{+}A_1(Q)^{-}$ state in the homodimeric reaction center core complex of *Heliobacterium modesticaldum*
   R. Miyamoto, H. Mino, T. Kondo, S. Itoh, and H. Oh-oka, (2008), *Biochemistry* 47, 4386–4393.

3. Temperature dependence of relaxation time of a stable radical pair in SyPixD investigated by pulsed EPR
   T. Kondo, S. Masuda, K. Tsutsui, H. Mino, (2011), *Chem. Phys. Lett.* 501, 528–533.

4. EPR study of 1Asp-3Cys ligated 4Fe-4S iron-sulfur cluster in NB-protein (BchN-BchB) of a dark-operative protochlorophyllide reductase complex
   T. Kondo, J. Nomata, Y. Fujita, and S. Itoh, (2011), *FEBS Lett.* 585, 214–218.

5. Interaction and inhibitory effect of ammonium cation in the oxygen evolving center of photosytem II
   M. Tsuno, H. Suzuki, T. Kondo, H. Mino, and T. Noguchi, (2011), *Biochemistry* 50, 2506-2514.

6. A heterogeneous tag-attachment to the homodimeric type 1 photosynthetic reaction center core protein in the green sulfur bacterium *Chlorobaculum tepidum*
   C. Azai, K. Kim, T. Kondo, J. Harada, S. Itoh, and H. Oh-oka, (2011), *Biochim. Biophys. Acta*, *in press.*

7. Pulsed EPR analysis of the photo-induced triplet radical pair in the BLUF protein SyPixD: Determination of the protein-protein distance and orientation in the oligomeric protein
   T. Kondo, S. Masuda, and H. Mino, (2011), *Appl. Magn. Reson.*, *submitted.*

8. Orientations of iron sulfur clusters in homodimeric type I photosynthetic reaction center of *Heliobacterium modesticaldum*
T. Kondo, M. Matsuoka, C. Azai, H. Mino, H. Oh-oka, and S. Itoh, *in preparation.*

9. Electron spin-polarized signal of the $P800^{+}A_1^{-}$(menaquinone^{-}) radical pair in type I reaction center of heliobacteria
T. Kondo, M. Matsuoka, C. Azai, H. Mino, H. Oh-oka, and S. Itoh, *in preparation.*

Acknowledgements

I would like to thank Dr. Hiroyuki Mino (Nagoya University) for his leadings, kind discussions, and significant suggestions about EPR measurements. I really thank Prof. Shigeru Itoh (Nagoya University) for his leadings, helpful discussions, and giving me the chance to study interesting subjects. I greatly thank Prof. Takumi Noguchi (Nagoya University) for providing me the opportunity for the study and Dr. Yutaka Shibata (Nagoya University) for helpful guidance regarding optical measurements and various discussions about curious topics in my field. I am deeply grateful to Dr. Hirozo Oh-oka (Osaka University) for significant comments and suggestions to accomplish my study on photosynthetic RC. I want to thank Dr. Yuichi Fujita (Nagoya University) for helpful advices about the study on DPOR enzyme and warm encouragements. I also deeply thank Dr. Shinji Masuda (Tokyo Institute of Technology) for sample preparations of BLUF protein and helpful guidance. My heartfelt appreciation goes to Mr. Masahiro Matsuoka (Osaka University) for his accomplished skills in the preparation of heliobacterial samples and kind encouragements. I am truly thankful to Dr. Jiro Nomata (Tokyo Institute of Technology) for sample preparation of DPOR enzyme and generous supports. I am sincerely grateful to Dr. Chihiro Azai (Osaka University) for insightful comments and productive discussions about a wide range of subjects. And, special thanks go to all members of Photobioenergetics Laboratory (G-lab) of Nagoya University.